

Review

The Future of Cancer Diagnosis, Treatment and Surveillance: A Systemic Review on Immunotherapy and Immuno-PET Radiotracers

Virginia Liberini ^{1,*}, Riccardo Laudicella ^{2,3}, Martina Capozza ⁴, Martin W. Huellner ³, Irene A. Burger ^{3,5}, Sergio Baldari ², Enzo Terreno ⁴ and Désirée Deandreis ¹

- ¹ Department of Medical Science, Division of Nuclear Medicine, University of Torino, 10126 Torino, Italy; desiree.deandreis@unito.it
- ² Department of Biomedical and Dental Sciences and of Morpho-Functional Imaging, Nuclear Medicine Unit, University of Messina, 98125 Messina, Italy; riclaudi@hotmail.it (R.L.); sergio.baldari@unime.it (S.B.)
- ³ Department of Nuclear Medicine, University Hospital Zurich, University of Zurich, 8006 Zurich, Switzerland; martin.huellner@usz.ch (M.W.H.); irene.burger@usz.ch (I.A.B.)
- ⁴ Molecular & Preclinical Imaging Centers, Department of Molecular Biotechnology and Health Sciences, University of Torino, Via Nizza 52, 10126 Torino, Italy; martina.capozza@unito.it (M.C.); enzo.terreno@unito.it (E.T.)
- ⁵ Department of Nuclear Medicine, Kantonsspital Baden, 5004 Baden, Switzerland
- * Correspondence: virginia.liberini@unito.it; Tel.: +39-0116335023
- † These authors contributed equally to this work.



Citation: Liberini, V.; Laudicella, R.; Capozza, M.; Huellner, M.W.; Burger, I.A.; Baldari, S.; Terreno, E.; Deandreis, D. The Future of Cancer Diagnosis, Treatment and Surveillance: A Systemic Review on Immunotherapy and Immuno-PET Radiotracers. *Molecules* **2021**, *26*, 2201. <https://doi.org/10.3390/molecules26082201>

Academic Editor: Amedeo Amedei

Received: 8 March 2021

Accepted: 9 April 2021

Published: 11 April 2021

Publisher's Note: MDPI stays neutral with regard to jurisdictional claims in published maps and institutional affiliations.



Copyright: © 2021 by the authors. Licensee MDPI, Basel, Switzerland. This article is an open access article distributed under the terms and conditions of the Creative Commons Attribution (CC BY) license (<https://creativecommons.org/licenses/by/4.0/>).

Abstract: Immunotherapy is an effective therapeutic option for several cancers. In the last years, the introduction of checkpoint inhibitors (ICIs) has shifted the therapeutic landscape in oncology and improved patient prognosis in a variety of neoplastic diseases. However, to date, the selection of the best patients eligible for these therapies, as well as the response assessment is still challenging. Patients are mainly stratified using an immunohistochemical analysis of the expression of antigens on biopsy specimens, such as PD-L1 and PD-1, on tumor cells, on peritumoral immune cells and/or in the tumor microenvironment (TME). Recently, the use and development of imaging biomarkers able to assess in-vivo cancer-related processes are becoming more important. Today, positron emission tomography (PET) with 2-deoxy-2-[¹⁸F]fluoro-D-glucose ([¹⁸F]FDG) is used routinely to evaluate tumor metabolism, and also to predict and monitor response to immunotherapy. Although highly sensitive, FDG-PET in general is rather unspecific. Novel radiopharmaceuticals (immuno-PET radiotracers), able to identify specific immune system targets, are under investigation in pre-clinical and clinical settings to better highlight all the mechanisms involved in immunotherapy. In this review, we will provide an overview of the main new immuno-PET radiotracers in development. We will also review the main players (immune cells, tumor cells and molecular targets) involved in immunotherapy. Furthermore, we report current applications and the evidence of using [¹⁸F]FDG PET in immunotherapy, including the use of artificial intelligence (AI).

Keywords: immune checkpoint inhibitors; immune checkpoint radiolabeled antibodies; PD-1; PD-L1; immune PET; immunotherapy; AI; radiomics; deep learning; CAR-T cells

1. Introduction

The origins of immunotherapy date back to the discovery of smallpox vaccination by Edward Jenner in 1796. Scientific interest in the mechanisms of immune surveillance of diseases has been high since then. In the last years, several findings on the involvement of both innate and adaptive immunity in the mechanisms of immune surveillance of cancer led to the emergence of immunotherapy, which is today considered one of the most promising anti-cancer approaches [1]. The knowledge of the complex and dynamic interactions between a tumor and the immune system has been fundamental for the development

of increasingly specific, personalized and targeted therapies. This was facilitated by the progress of modern medicine through increasing multidisciplinary and translational approaches, including omics sciences (e.g., genomics, proteomics, metabolomics). The same knowledge is also exploited by the growing field of molecular imaging through the identification of diagnostic biomarkers to support clinical decision-making and patient selection by non-invasive, in-vivo assessment of specific therapy target expression, therapy response and toxicity. In recent years, also technological development assumed an important role in supporting clinical decision-making and selecting patients as immunotherapy candidates. First, new digital tomographs have greatly improved the detectability of small lesions, but also the use of artificial intelligence (AI), may improve the interpretation of so-called “big-data” extracted from images and allow for their integration with other medical data. Here, we will review the state of the art and the perspectives in the aforementioned aspects in the field of immunotherapy, with a special focus on molecular imaging.

2. Material and Methods

We searched the PubMed, PMC, Scopus, Google Scholar, Embase, Web of Science, and Cochrane library databases (between January 2015 and February 2021), using the following both as text and as MeSH terms: “immunotherapy”, “ICI*”, “PET”, “micro-PET”, “PET/CT”, “PET/MR”, “convolutional”, “neural”, “network”, “machine”, “learning”. No language restriction was applied to the search, but only articles in English were reviewed. The systematic literature search returned 822 articles. According to the PRISMA flow-chart, after duplicate removal, 86 articles have been considered, fully read, analyzed, and extensively described according to their title and abstract as previously described [2]. We also checked for further relevant articles in the references of the articles included in the retrieved literature.

3. Tumor Microenvironment

As recently observed, cancer should not be considered as a simple collection of transformed cells, but as an organic and evolving complex of transformed tumor cells and other cellular and molecular components that together constitute the *tumor microenvironment* (TME) [1], as illustrated in Figure 1.

On the one hand, tumor cells and stromal cells, such as cancer-associated fibroblasts (CAFs), adipocytes, and vascular endothelial cells, co-evolve and grow within a protective extracellular matrix (ECM) with the help of cytokines, glycoproteins, proteoglycans and growth factors. On the other side, tumor-infiltrating immune cells present in the TME try to identify and destroy growing tumor cells. This defensive behavior may also be associated with tissue inflammation and a pro-tumorigenic effect responsible for the selection of more aggressive tumor clones, able to block and evade the same immune defensive mechanism [3]. The two major players of the anti-tumorigenic effect of the immune system are the natural killer (NK) cells and the tumor-infiltrating lymphocytes (TILs), which recognize and kill the tumor cells through different mechanisms. First NK cells target cells that do not present the major histocompatibility class I (MHC-I) on their surface. Once activated, NK cells release cytolytic granules to trigger programmed cell death. Differently, CD8⁺ T-lymphocytes and CD4⁺ T helper lymphocytes 1 (Th1) are activated by antigen-presenting cells (APCs), such as dendritic cells (DCs), but also by mononuclear phagocytes and B cells. The APCs can recognize and capture extracellular proteins from tumor cells and present them as antigen-derived peptides to CD4⁺ and CD8⁺ T-lymphocytes by the major histocompatibility complex molecules of class I and II (MHC-I and MHC-II) expressed by these cells; this is a critical step for an effective adaptive immune response [4]. Moreover, CD4⁺ Th1 T-lymphocytes destroy tumor cells also through the secretion of cytokines and chemokines, especially interleukin 2 (IL2) and interferon-gamma (IFN γ), which help the recruitment of further NK cells, CD8⁺ T-lymphocytes and macrophages. These mechanisms also prevent metastatic spread of the tumor [5].

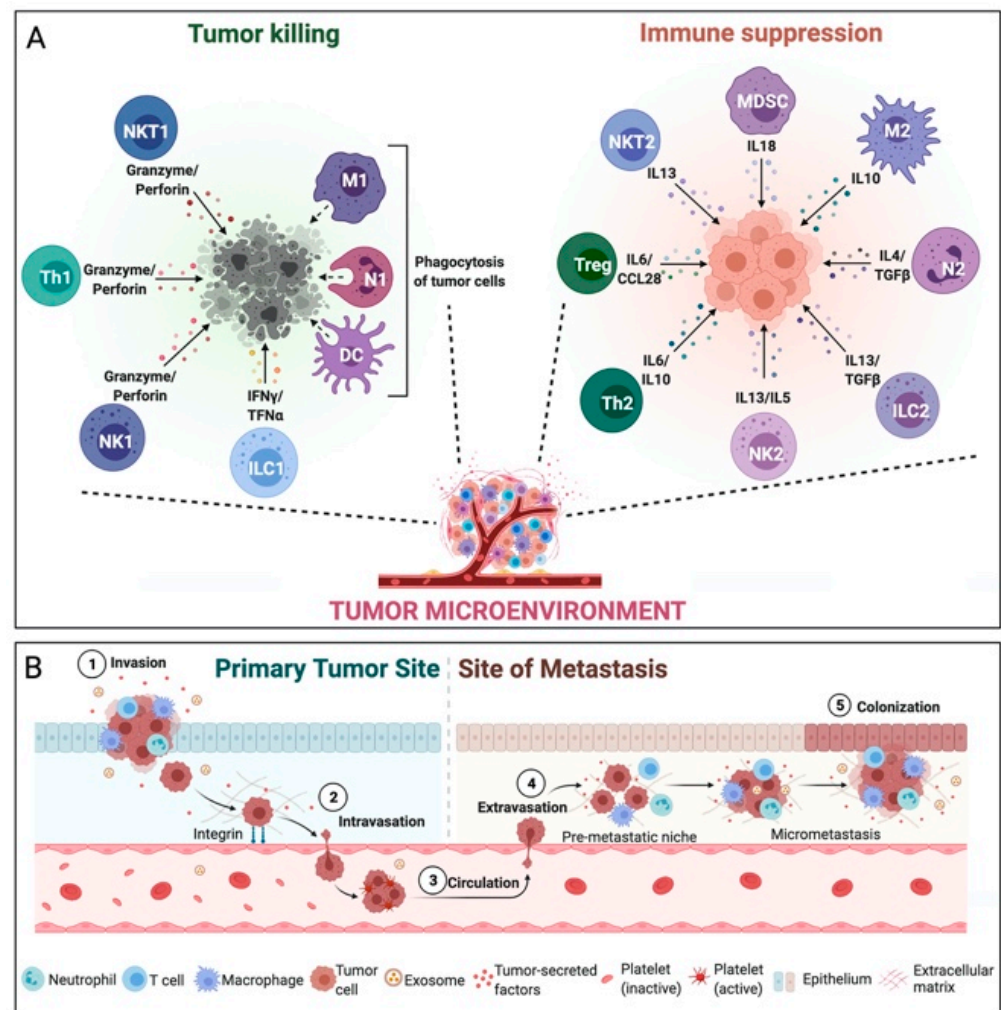


Figure 1. Simplified schematic representation of the tumor microenvironment. (A) Schematic representation of immune cells in tumor microenvironment that have an anti-tumorigenic effect (natural killer and tumor-infiltrating lymphocytes) and of other tumor-infiltrating immune cells that have a pro-tumorigenic effect ($CD4^+$ T helper lymphocytes 2 (Th2), the regulatory $CD4^+$ T-lymphocytes (Treg)). (B) schematic representation of immune cells role in tumor spreading process.

Second, tumor-infiltrating immune cells play a more ambivalent role and may as well have an anti-tumorigenic or a pro-tumorigenic effect based on a delicate balance of different mechanisms within the TME. Namely, other TILs can exhibit a pro-tumorigenic effect, such as $CD4^+$ T helper lymphocytes 2 (Th2), producing interleukins with an inflammatory effect, and the regulatory $CD4^+$ T-lymphocytes (Treg), which are indispensable for maintaining homeostasis, down-regulating the $CD8^+$ T-lymphocyte activity [1,6]. Also, the presence of tumor-associated macrophages (TAMs) is related to a poor prognosis and reduced overall survival (OS). TAMs phenotype can be polarized by the TME characteristics, resulting in the development of pro-inflammatory macrophages (M1 type, driven by $IFN\gamma$ and tumor necrosis factor- α (TNF α) or anti-inflammatory macrophages (M2 type, driven by IL4 and IL13). While the former ones have an anti-tumorigenic effect, the latter ones promote tumor progression by stimulating angiogenesis, remodeling the ECM, promoting metastasis and immunosuppression [1,3,5,7,8]. Tumor-associated neutrophils (TANs) may also show a similar behavior: they can be polarized, resulting in the development of an anti-tumorigenic type (N1) or a pro-tumorigenic type (N2). Driven by the action of transforming growth factor- β (TGF- β) secreted by the CAFs, N2 stimulate cancer proliferation and migration through the secretion of matrix metalloproteinases (MMPs) and IL1 β [3,4,9]. Finally, the role of tumor-infiltrating B cells (TIBs) is even more controversial: $CD20^+$ TIBs

have been shown to behave as APCs with an anti-tumorigenic effect in non-small-cell lung cancer (NSCLC), ovarian cancer [10,11] and in melanoma, as part of the tertiary lymphoid structures (TLS) associated with CD8⁺ T-lymphocytes [12]. Moreover, CD20⁺ TIBs can produce granzyme B and perforin, which directly leads to the activation of apoptotic pathways in tumor cells. In contrast, however, Shalapour et al. demonstrated that TIBs seem to inhibit the anti-tumorigenic effect of CD8⁺ T-lymphocytes, promoting tumor cell growth and migration [13].

4. Immunotherapies Targets

The understanding of the complex mechanisms regulating immune cell infiltration in the TME is still evolving. A comprehension of this intricate system is crucial in order to develop new immunotherapy strategies for cancer treatment, such as immune checkpoint inhibitors (ICIs), adoptive cell transfer (ACT), oncolytic virus therapies, cancer vaccines and cytokine therapies (Figure 2).

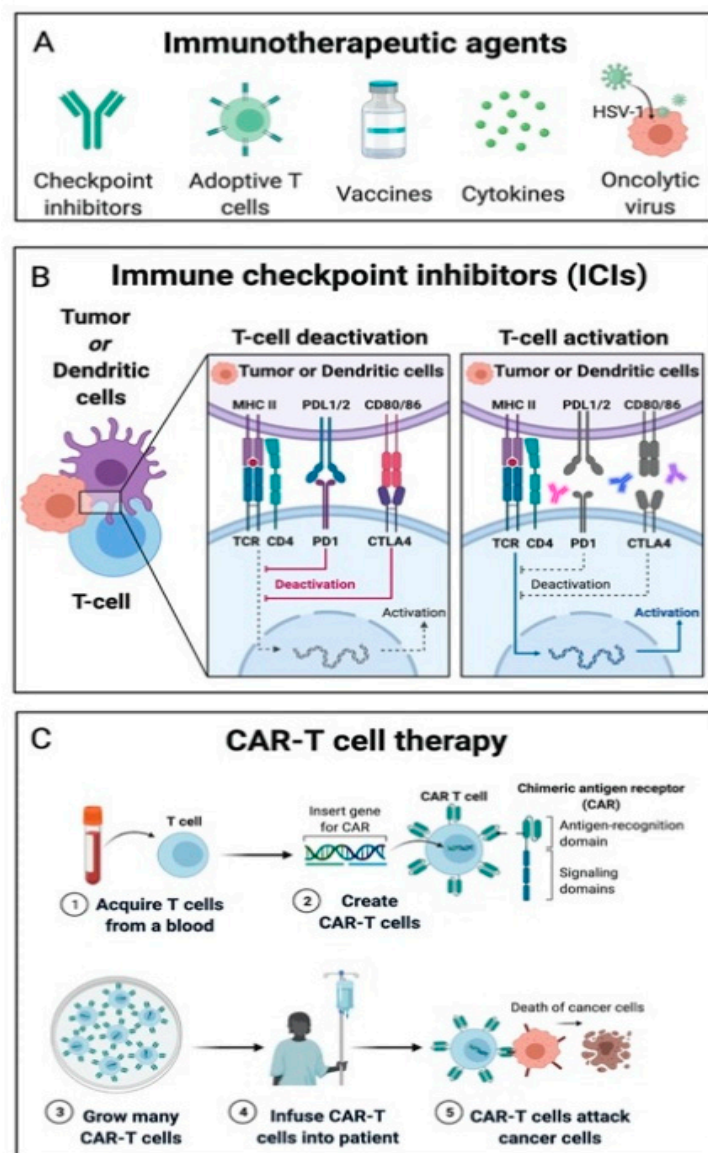


Figure 2. Simplified schematic representation of the new immunotherapy strategies for cancer (A), with particular attention to the most widely used immunotherapies: the Immune Checkpoint Inhibitors (B) and the CAR-T Cell Therapy (C).

4.1. Immune Checkpoint Inhibitors

ICIs are nowadays the most commonly used immunotherapy strategy. ICIs represent a class of monoclonal antibodies (mAbs), able to counteract the immunosuppressive action of the immune checkpoint (IC) proteins and re-establishing the anti-tumorigenic function of the tumor-infiltrating immune cells present in the TME [1,3,5,14]. As the above-mentioned Treg, ICs are fundamental for maintaining homeostasis, down-regulating CD8⁺ T-lymphocyte activity, and for preventing autoimmune reactions [15]. Cancer cells have learned to take advantage of this mechanism, producing and overexpressing ICs on their cell surface and down-regulating the immune system [16]. Cytotoxic T-lymphocyte associated protein 4 (CTLA-4), programmed cell death protein 1 (PD-1) and its ligands (PD-L1 and PD-L2) are the protagonists of this process. CTLA-4 is a glycoprotein expressed on the T cell surface, which allows tumor cells to escape the immune system by binding to CD80/86 on APCs. Anti-CTLA-4 therapies, such as ipilimumab, block this mechanism [17]. Furthermore, tumor cells can express PD-L1 and PD-L2 on their surface, thereby blocking the activity of T cells, B cells and NK cells, binding their surface receptor PD1. Anti-PD1 therapies, such as nivolumab and pembrolizumab, and anti-PD-L1 therapies, such as avelumab, atezolizumab and durvalumab block this mechanism [18].

4.2. Adoptive Cell Transfer

Another widely used immunotherapy technique is the adoptive cell transfer (ACT), whose main representatives are chimeric antigen receptor (CAR)-T cells. CAR-T cells are autologous isolated T cells, genetically engineered through the use of antibody fragments to carry a receptor capable of recognizing specific antigens expressed by tumor cells, being reinfused to patients to stimulate cancer immune surveillance through secretion of perforin and granzyme granules and activation of programmed cell death.

CARs have been categorized into four generations according to the number of intracellular signaling molecules: while the first-generation CAR-T cells induced immune system reaction against target cancer cells, but could not promote CAR-T cells expansion in-vivo following reinfusion (could be reproduced only ex-vivo), on the other hand, other generations of CAR-T cells contained additional intracellular co-stimulatory domains, which allowed these CAR-T cells to grow, expand and ultimately be persistent in the patient's body [19–21].

CAR-T cells were developed for the treatment of hematologic disorders, such as acute lymphoblastic leukemia (ALL) and chronic lymphocytic leukemia (CLL) in adult patients [22–24]. Their use for solid cancer is still challenging due to the higher heterogeneity of tumoral antigens, the resulting increased difficulty in configuration recognition, higher difficulty to penetrate tumor tissue through the vascular endothelium and a low survival in the TME [21].

4.3. Oncolytic Viruses, Cancer Vaccines and Cytokine Therapies

Another immunotherapy technique uses oncolytic viruses described as modified viruses aimed to target and kill tumor cells. In 2015, the Food and Drug Administration (FDA) approved talimogene laherparepvec (T-Vec), also known as Imlygic[®], the first oncolytic modified herpes simplex virus, that infects and destroys melanoma cells in patients with unresectable metastatic disease [25,26].

Cancer vaccines are another approach in immunotherapy, relying on tumor-specific antigens to trigger T-cell activation in the TME. Its largest field of application is melanoma (MZ2-E, MZ2-D and gp100 antigens [27–29]), but this technique has also been used in prostate cancer (sipuleucel-T, a dendritic cell-based cancer vaccine [30]).

Despite the efficacy and initial enthusiasm for the use of cytokine therapies, especially in patients with chronic myeloid leukemia and melanoma, IL2 and TNF α have recently been sidelined in favor of the abovementioned more promising ICIs and ACT approaches, owing to their poor tolerability and severe toxicity [1,3,5,14].

4.4. Open Question on the Use of Immunotherapies Targets

Among all the aforementioned immunotherapy-based treatment, ICIs appear to be the most rapidly evolving ones. Since the first publication on the use of ipilimumab in a clinical trial in patients with metastatic melanoma in 2010 [31], ICIs have been approved by the FDA for the treatment of several cancer types besides malignant melanoma, such as renal cell carcinoma, squamous cell carcinoma of the head & neck, Merkel cell carcinoma, hepatocellular carcinoma, cervical cancer, small-cell lung cancer, non-small-cell lung cancer, triple-negative breast cancer, gastric carcinoma, urothelial cancer and Hodgkin lymphoma [32].

However, only a subset of patients responds to immunotherapy, with a very heterogeneous response rate depending on ICIs and cancer type [33–36]. Moreover, immunotherapy is not exempt from autoimmune-like reactions and immune-related adverse events (irAEs), such as skin rash, pneumonitis, colitis, hepatitis and thyroiditis, that occur in approximately 50% of patients overall, and in 14% as grade 3–4 side effect, according to the Common Toxicity Criteria for Adverse Events (CTCAE) [18].

The exact reasons for response heterogeneity, tumor relapse and side effects are still not clear. A high immunohistochemical (IHC) staining of PD-L1 tumor expression [37,38] and/or PD-1 and CTLA-4 TILs expression [39] on biopsy specimens is the first fundamental step for treatment selection, being generally but not only related to higher response rate to ICI therapy. However, evaluation of ICs expression is generally assessed by a single-tumor biopsy, leading to its potential underestimation [40], as tumor heterogeneity is both spatial (inter- and intra-tumoral heterogeneity of ICs expression) and time-related (more aggressive cell clones developing over time) [41,42]. Thus, while multiple-lesion biopsy sampling is not feasible most of the time, grading heterogeneity among primary and metastasis would be a valuable approach through whole body target expression techniques.

In clinical practice, the indication for treatment with ICIs is based on the expression of ICs on tumor, assessed on the histological sample of the tumor. Patient selection criteria for therapy with ICIs (percentage of expression of ICs) vary depending on the tumor under investigation and the drugs considered. However, a good overall survival after treatment with ICIs was surprisingly found even in patients with low PD-L1 expression (PD-L1 expression of 1%) on the biopsy sample. For this reason, new criteria for the selection of patients who could benefit from these therapies have been recently evaluated. In particular, the combined positive score (CPS) has been introduced, a composite of ICs (such as PD-L1) tumor proportion score (TPS) and host- and tumor-related parameters, which evaluates the percentage of positive ICs (tumor cells, lymphocytes and macrophages) present in the TME [43,44].

5. Molecular Imaging

Non-invasive *in vivo* imaging techniques, such as computed tomography (CT), magnetic resonance imaging (MRI), positron emission tomography (PET) and single-photon emission computed tomography (SPECT) as single or hybrid modalities (i.e., PET/CT, PET/MRI, SPECT/CT) may provide valuable information for staging, patient selection, treatment response assessment, restaging and follow-up, even though optimal biomarkers to predict immunotherapy response and toxicity have not been identified yet [34].

5.1. Immuno-PET

5.1.1. Critical Issues in the Development of a Good Radiotracer in Immunotherapy

The development of a new molecular imaging probe to answer a specific biological question is a complex process, that requires a multidisciplinary team, significant funds and several decisional stages from the laboratory bench to animal models, and from animal models to the clinic. A good molecular probe needs to overcome biological problems, such as rapid clearance, metabolism, degradation and too early excretion, non-specific accumulation in non-target tissues, poor perfusion of the tumor and pharmacological delivery barriers [45]. Also, further potential issues related to radioactive decay and toxicity

have to be considered. Ideally, the radiotracer: (1) must be composed of a radioactive isotope with an identical behavior as the stable isotopes of the same element, (2) must not change the chemical and physical properties of the biological system in which it will be introduced, (3) must not deviate the normal physiological state of the system under consideration, (4) must be highly specific and/or selective, with high plasma clearance and low plasma protein binding, (5) must have the same chemical and physical characteristics of the unlabeled compound, (6) must have good in-vivo stability, the labelling between the radionuclide and the compound must be strong enough to avoid the detection of free radionuclide, and (7) must have a blood half-time adequate to the specific biological question [46,47].

New radiotracers have been developed in the field of immunotherapy, using both ex-vivo or in-vivo labelling methods. Ex-vivo cell labeling techniques are currently increasing. Here, immune cells are isolated from a patient and incubated with the radionuclide ex-vivo, despite the high fragility (short viability) of the re-injected cells and only preclinical data available, till now. An in-vivo approach would allow the possibility of PET imaging at any time after cell infusion, especially this could be of particular interest in the case of CAR T cell infusion, allowing to verify their arrival and accumulation in the tumor and metastases rather than a simple assessment of their presence in the peripheral blood by serial sampling, as per current procedural lines [48]. The first trials were carried out using SPECT radionuclides, such as [^{99m}Tc] labeled hexamethylpropyleneamine (HMPAO) or [^{111}In] labeled 8-hydroxy-quinoline (oxine). In 2003, Meidenbauer et al. [49] labeled Melan-A-specific CD8⁺ cytotoxic T lymphocytes with [^{111}In]oxine and demonstrated the localization of these radiolabeled cells to metastatic sites 48 h after injection [49]. More recently, several groups [50–52] have studied ex-vivo CAR-T cells labeling techniques using [^{89}Zr] for PET imaging. The synthesis and labelling steps are similar to those used for the [^{111}In]oxine complex, but the use of [^{89}Zr] is more promising, owing to the higher spatial resolution, higher sensitivity, and better signal-to-background ratio of PET compared with SPECT, and owing to its comparably long half-life of 3.27 days compared to 2.80 days for ^{111}In , which is helpful to monitor cell distribution in murine models after administration [53]. However, the efflux of [^{89}Zr] is the major drawback of this radionuclide, owing to the high radiotoxicity exhibited by free [^{89}Zr]. This problem has been solved by Bansal et al., which covalently labeled [^{89}Zr] to cell surface proteins of mouse-derived melanoma cells, mouse dendritic cells and human mesenchymal cells, although only 30–50% of the cells were found to be efficiently bound [50]. In-vivo labeling techniques have been easier to implement and are in more advanced research phases with some clinical applications, already. In particular, radionuclide-labeled immunoglobulins G (IgG) antibodies (mAbs), antibody fragments or small proteins may be used to detect in-vivo the expression of ICs (PD-L1, PD-1 and CTLA-4), and/or other key molecules of immune checkpoint pathways and immune responses through SPECT or PET/CT images [15]. The choice of the right antigen expressed only on target cells with the right radionuclide is fundamental to create a good radiotracer: [^{111}In], [^{89}Zr] and [^{64}Cu] with longer half-lives (67.2, 78.4 and 12.7 h, respectively) are better suited to label intact antibodies (mAbs), while [^{18}F] and [^{68}Ga] with shorter half-lives (109.8 and 67.7 min, respectively) are more suitable for labeling of smaller ligands, such as nanobodies or small proteins [48,54]. The key radionuclides used for the development of new radiotracers in the immunotherapy field are listed in Table 1.

Full-length antibodies (IgG, mAbs) are large proteins with a molecular weight >150 kDa, resulting in low tumor infiltration and long blood half-life: indeed, they are eliminated in two or three weeks by either excretion (being filtered, reabsorbed and metabolized through proximal tubule of the nephron) or catabolism (through intracellular catabolism by lysosomal degradation to amino acids after uptake by pinocytosis or by a receptor-mediated endocytosis process). This demands the use of long physical half-life radionuclides increasing patient's radiation exposure and requiring image acquisition up to one week after injection. On the contrary, antibody fragments and small proteins are preferred over

IgG/mAbs due to their shorter biological half-life. In fact, unbound molecules are rapidly cleared from the circulation through kidney excretion, resulting in high-contrast images with improved tumor-to-background signal ratio [55]. This phenomenon allows the use of shorter half-life radionuclides, such as [¹⁸F] and [⁶⁸Ga], which are already widely used in clinical practice, and where images are acquired earlier (after 1–2 h), which is a big advantage in clinical routine. Another significant advantage of using smaller imaging agents is their faster diffusion and better penetration, compared to the heavier full-length IgG/mAbs, into dense solid tumors, leading to better intra-tumoral distribution [56,57].

Table 1. Characteristics of key radionuclide use for the development of new radiotracer in the immunotherapy field.

Radionuclide	Half-life	Type of Emission	Energy of Emission (keV)	Particle Maximum Range in Water
[¹¹ C] (carbon)	20.4 min	β+	970	3.67 mm
[⁶⁸ Ga] (gallium)	67.7 min	β+	1900	9.06 mm
[¹⁸ F] (fluorine)	109.7 min	β+	640	2.16 mm
[⁶⁴ Cu] (copper)	12.7 h	β+ (19%) β− (38%) γ (43%)	657 141 511 and 1346	≈ 2 mm
[⁸⁹ Zr] (zirconium)	3.27 d	β+	909	≈ 3 mm

Another interesting new option is the use of bispecific antibodies, which are able to bind both endogenous T cells (binding especially CD3 on T cells) and tumor-specific antigens, bringing them into close proximity and facilitating the induction of immune cell mediated apoptosis [58]. However, the mechanisms of function of these bispecific antibodies are unclear and in particular it is difficult to understand whether these antibodies have higher affinity for tumor cells or T cells and consequently it is difficult to predict their biodistribution. Molecular imaging could accelerate the development of these drugs by obtaining information on biodistribution and target involvement using radiolabeled bispecific antibodies.

Finally, the chelator is also critical to prevent dissociation of the radionuclide from the compound, as is often the case with [⁶⁴Cu], which tends to accumulate in the liver when it dissociates from the chelator [59].

Among all the new immune-cancer related radiotracers created in recent years, those associated especially with immune checkpoints and adoptive cell transfer techniques, and those targeting CD8+ T lymphocytes, which seem to have the most important anti-tumorigenic role in the TME, are the most promising ones. All the radiotracers tested in clinical trials are listed in Table 2.

Table 2. Most relevant radiotracers tested in clinical trials.

Targeting Molecule	Agent	Molecule Type	Tumor Model	Stage	Reference
	[¹⁸ F]BMS-986192	adnectin	NSCLC patients	clinical	[60]
PD-L1	[⁸⁹ Zr]-labeled atezolizumab	antibody IgG1	metastatic bladder cancer, NSCLC, or triple-negative breast cancer	clinical	[61]
PD-1	[⁸⁹ Zr]nivolumab	antibody IgG4	NSCLC patients	clinical	[60]
CD8+	[⁸⁹ Zr]Df-IAB22M2C	minibody	melanoma, lung cancer, and hepatocellular carcinoma	clinical	[62]

5.1.2. PD-1/PD-L1 Pathways

As mentioned above, PD-1/PD-L1 pathway is the most widely used immunotherapeutic approach, being also the most studied pathway in pre-clinical and clinical studies. However, different targets, such as antibodies and small molecules, have been considered to identify a good radiotracer.

Labelled Antibodies

Since the development of the first [^{64}Cu]DOTA labeled antibody (IgG) PD-1 radiotracer by Natarajan et al. [63] in 2015, being tested on mice bearing B16-10 melanoma tumors, several immune checkpoint radiotracers have been developed both for SPECT and PET imaging. The development of these radiotracers required some changes in the mice-model used in the preclinical laboratory: immunodeficient mice commonly used to study xenograft tumor models do not provide important information on radiotracer distribution in healthy organs, such as liver, spleen, thymus, lung and brown fat. Therefore, immunocompetent mice have been developed to allow studying both tumor and healthy tissue distribution of these new radiotracers [64]. In 2016, Nedrow et al. studied the in-vivo biodistribution of [^{111}In]diethylenetriaminepentaacetic acid (DTPA)-anti-PD-L1 antibody in an immunocompetent murine model of melanoma. Authors reported how splenic uptake of the radiotracer affected the tumor uptake and how the co-injection of labeled antibodies and 100-fold of unlabeled antibodies significantly reduced splenic uptake of the radiotracer at 24 h, shifting the concentration of [^{111}In]DTPA-anti-PD-L1 in the blood and potentially increasing tumor uptake [65]. Owing to these results, the assessment of the influence of the cold antigen on radiotracer accumulation in the tumor has been introduced also in many other preclinical studies [66–68]. Several antigens have been studied for the development of PD-L1 radiotracers, including full-length IgG/mAbs, antibody fragments and small molecules, while only full-length IgG/mAbs have been used for the development of PD-1 radiotracers.

Interestingly, Kikuchi et al. [69] demonstrated that radiotherapy induced a PD-L1 upregulation in tumor, enhancing the efficacy of either treatment alone. They assessed a [^{89}Zr] labeled anti-mouse PD-L1 mAb and dynamic immuno-PET/CT imaging of two murine tumor models (head and neck squamous cell carcinoma and melanoma), alone and during anti-PD-1 mAb immunotherapy. PET/CT imaging demonstrated significantly increased radiotracer uptake in irradiated head and neck tumors compared with non-irradiated flank tumors, whilst anti-PD-1 therapy did not have the same effect.

Similar results have been proven also by Christensen et al. [70]. Authors studied the efficacy of the anti-PD-L1 (clone 6E11) conjugated with dibenzocyclooctyne-Desferrioxamine (DIBO-DFO) chelator and radiolabelled with [^{89}Zr] ([^{89}Zr]DFO-6E11) on NSCLC xenografts and syngeneic tumors models with different levels of PD-L1 in CT26 tumor-bearing mice subjected to external radiation therapy (XRT) in combination with PD-L1 blockade. [^{89}Zr]DFO-6E11 detected the differences in PD-L1 expression among tumor models and quantified the increase in PD-L1 expression in tumors of irradiated mice.

Radiolabeled Small Molecules

Several small molecules have been studied to overcome the aforementioned problems related to the use of full-length mAbs. Gaochao et al. [71] designed and developed [^{68}Ga] labeled single-domain antibody radiotracer, [^{68}Ga]NOTA-Nb109, for specific and non-invasive imaging of PD-L1 expression in a melanoma-bearing mouse model. Also, Rubins et al. [72] evaluated the PD-L1-targeting affibody molecule ZPD-L1_1 as a PET radiotracer in a mouse tumor model of human PD-L1 expression, radiolabeled with either [^{18}F]AIF-NOTA or [^{68}Ga]NOTA.

In 2017, Chatterjee et al. [59] produced a PET radiotracer labeling the [^{64}Cu]DOTAGA with the WL12 peptide, able to bind PD-L1 with high affinity (half maximal inhibitory concentration (IC₅₀) \approx 23 nM). They evaluated the ability of [^{64}Cu]DOTAGA-WL12 to detect PD-L1 expression in-vivo by PET imaging in NSG (non-obese diabetic (NOD) scid

gamma) mice, immunodeficient laboratory mice, harboring Chinese hamster ovary (CHO) tumors with constitutive human PD-L1 expression (hPD-L1) and isogenic negative control tumors. The radiotracer was able to early detect tumor PD-L1 expression, within 60 min after administration, however, with increased uptake in the liver due to the dissociation of Cu²⁺ from the chelator and its subsequent trans-chelation to plasma proteins, such as albumin and ceruloplasmin. Thereafter, Ravindra et al. [73] studied the WL12 peptide labeling with [⁶⁸Ga]DOTAGA. In immunocompetent mice, the percentage of injected dose per gram (%ID/g) at 60 min resulted much higher in hPD-L1 cells (11.56 ± 3.18), with better tumor-to-background contrast, compared to other cell lines (<4.97). Moreover, the uptake of [⁶⁸Ga]DOTAGA-WL12 in the liver was 50–90% less compared to [⁶⁴Cu]DOTAGA-WL12. Finally, Lesniak et al. [74] evaluated the novel [¹⁸F]FPy-WL12 radiotracer both in-vitro, in six cancer cell lines with varying PD-L1 expression, and in-vivo, where high liver and kidney uptake indicated the need for an optimized labeling strategy to improve the in vivo pharmacokinetics of the radiotracer.

Still in 2017, Meyer et al. [75] used a small high-affinity engineered protein scaffold (HAC-PD1) to create six different HAC-PD1 radiotracer variants based on the use of different chelate, glycosylation, and radionuclide, tested on mice-models with tumors engineered to either be constitutively positive (CT26 hPD-L1) or negative (DmPD-L1 CT26) for human PD-L1 expression. All radiotracers showed an early (60 min) detection of the PD-L1 positive tumors and [⁶⁸Ga]NOTA-HACA-PD1 and [⁶⁸Ga]DOTA-HACA-PD1, the most suitable candidates for translation into the clinic, exhibited promising target-to-background ratios in ex-vivo biodistribution studies.

In 2018, Truillet et al. [76] developed a [⁸⁹Zr]desferrioxamine B (DFO) radiolabeled recombinant human IgG1 (C4) that specifically binds PD-L1. Authors showed how [⁸⁹Zr]DFO-C4 detected PD-L1 antigen on human NSCLC models and prostate cancer models endogenously expressing a broad range of PD-L1 with a linear positive correlation to the grade of PD-L1 tumor expression. The best tumor-to-background contrast was obtained at 48 h after injection. They also demonstrated how standard chemotherapy changed PD-L1 expression on tumor cells and consequently also changed [⁸⁹Zr]DFO-C4 uptake, underscoring the potential utility of serial imaging to measure clinically relevant expression changes over time.

Further, a study performed by Xu et al. [77] compared a novel anti-PD-L1 antibody radiotracer ([⁶⁴Cu]NOTA-MX001) uptake with [¹⁸F]FDG uptake in mice bearing MC38 (PD-L1 positive) and 4T1 (PD-L1 negative) xenografts. Interestingly, the uptake of [¹⁸F]FDG in MC38 and 4T1 xenografts was 5.3 ± 0.4 and 6.4 ± 0.6%ID/g at 1 h, while the uptake of [⁶⁴Cu]NOTA-MX001 was 5.6 ± 0.3 and 1.3 ± 0.4%ID/g at 12 h, allowing to verify the tumor's expression of PD-L1 in contrast to nonspecific [¹⁸F]FDG uptake.

In 2019, Wissler et al. [78] developed a site-specific αPD-L1 antigen-binding fragment (Fab) conjugate with [⁶⁴Cu]NOTA ([⁶⁴Cu]NOTA-αPD-L1) for effective and early visualization and mapping of the biodistribution of PD-L1 in two normal mouse models, which could facilitate the elucidation of the roles of a wide variety of immune checkpoint proteins in immunotherapy at 5, 15, and 45 min post-injection. In the same year, Li et al. [79] evaluated [⁸⁹Zr]Df-KN035, the first 79.6 kDa size anti-PD-L1 domain antibody (KN035), to monitor PD-L1 levels in nude mice bearing LN229 xenografts (brain cancer) with a positive expression for PD-L1. They found that LN229 xenografts were markedly visualized from 24 h after injection of [⁸⁹Zr]Df-KN035, with high uptake enduring up to 120 h with a favorable tumor-to-muscle ratio. The same group also evaluated the impact of chemotherapy, radiotherapy or epidermal growth factor receptor (*EGFR*) tyrosine kinase inhibitor (TKIs) effect on the TME (PD-L1 levels) of NSCLC. PET imaging with [⁸⁹Zr]Df-KN035 was performed before and after *EGFR*-TKI gefitinib treatment to evaluate PD-L1 expression, observing that the high dose of gefitinib inhibited tumor growth and decreased the tumoral uptake of [⁸⁹Zr]Df-KN035 [80].

Finally, another [¹⁸F]labeled small molecule inhibitor, [¹⁸F]LN, was designed in 2020 by Yinxing et al. [81] to evaluate PET imaging in both PD-L1 transfected (A375-hPD-L1)

and non-transfected (A375) melanoma-bearing mice. Authors observed that tumor uptake (1.96 ± 0.27 %ID/g) reached the maximum at 15 min in the positive group, being 2.2-fold higher than in the negative (0.89 ± 0.31 %ID/g) or the blocked (1.07 ± 0.26 %ID/g) group.

Radiolabeled Atezolizumab

Other anti-PD-L1 mAbs have been investigated in several clinical trials, such as [^{89}Zr]avelumab in a breast cancer mice-model [66] and the promising [^{89}Zr]DFO-atezolizumab in a human tumorgraft model. In 2019, Vento et al. [82] showed for the first time the expression of PD-L1 in a renal cell carcinoma removed from a patient (with favorable nivolumab response) and implanted orthotopically into NOD/SCID mice. This was demonstrated using in-vivo PET images of atezolizumab (monoclonal anti-PD-L1 antibody with a mutant Fc) radiolabeled with [^{89}Zr]DFO. Also in 2019, Bensch et al. [61] presented the first-in-human study of [^{89}Zr]atezolizumab immune-PET in 22 patients with metastatic bladder cancer, NSCLC, or triple-negative breast cancer. They found a better correlation between progression-free survival (PFS) and OS with pre-treatment radiotracer uptake, compared to conventional IHC staining of PD-L1. These findings highlight the limitations of a single biopsy evaluation and show the benefit of in-vivo assessment by imaging. As in preclinical studies, 10 mg of unlabeled atezolizumab was administered together with the radiotracer to prevent rapid clearance during imaging, which was performed on days 4 and 7. Physiological biodistribution has been reported as following: low uptake in healthy brain, subcutaneous tissue, muscle, compact bone, and lung; higher uptake (increasing over time) in bone marrow, intestines, kidney, and liver. Overall, the observed [^{89}Zr]atezolizumab uptake in lymphoid tissue (lymph nodes and spleen mainly) might serve as a surrogate for the activation state of the body's immune system or as a measure for abundant PD-L1 expression. Tumor [^{89}Zr]atezolizumab uptake was generally high, with an overall geometric mean SUV_{max} of 10.4, but often with a heterogeneous intratumoral, intertumoral and interpatient radiotracer distribution.

Radiolabeled Pembrolizumab

In 2020, different targets have been individualized for the development of new immuno-PET radiotracers imaging PD-1 expression. In-vivo pharmacokinetics and whole-body distribution of [^{89}Zr]labeled PD-1 targeting pembrolizumab with PET in humanized mice have been recently studied by van der Veen et al. [83], with disappointing results: tumor uptake of [^{89}Zr]pembrolizumab was lower than uptake in normal lymphoid tissue, but higher compared to other organs. High uptake in lymphoid tissues (such as spleen, lymph nodes and bone marrow) was reduced by excess unlabeled pembrolizumab administration, which inversely did not affect tumor uptake. Instead, Wenping et al. [84] evaluated the biodistribution of [^{89}Zr]labeled pembrolizumab, a humanized IgG4 kappa monoclonal antibody targeting PD-1, in healthy cynomolgus monkeys as a translational model of tracking PD1-positive immune cells with better results: distribution in lymphoid tissue such as mesenteric lymph nodes, spleen, and palatine tonsils increased over time, although it was reduced when a large excess of cold pembrolizumab was co-administered with the radiotracer. Moreover, except for the liver, low radiotracer distribution was observed in all non-lymphoid tissues including lung, muscle, brain, heart, and kidney.

Radiolabeled Nivolumab

The early studies with nivolumab were fraught with problems. Similarly to [^{64}Cu]DO-TAGA-WL12, Cole et al. [85] reported the presence of consistent high liver uptake concerning the in-vivo distribution of [^{89}Zr]labeled nivolumab in healthy non-human primates (NHP), but also the possibility to block splenic uptake by co-administration of excess cold nivolumab. England et al. [86] developed another [^{89}Zr]nivolumab radiotracer labeled with p-SCN- DFO chelator and a humanized murine model of lung cancer suitable for immuno-PET images. However, in their study, a proper accumulation of [^{89}Zr]Df-nivolumab was not reached before 48 h, and uptake values were calculated at 168 h post-injection; more-

over, salivary gland and splenic uptake could be another potential complication for proper image interpretation.

In 2018, Niemeijer et al. [60] reported the first-in-human study using whole-body PET imaging with [⁸⁹Zr]nivolumab (anti-PD-1) and [¹⁸F]BMS-986192, an [¹⁸F]labeled anti-PD-L1 fibronectin-based protein (adnectin), in 13 patients with advanced NSCLC before treatment with nivolumab. Acquisition time was 7 days after administration of [⁸⁹Zr]nivolumab, reflecting PD-1-expressing tumor-infiltrating immune cells, and 1 h after injection of [¹⁸F]BMS-986192, reflecting PD-L1 expression in tumor lesions. Both radiotracers showed favorable distribution in tumor, but with a high heterogeneity between patients and lesions, and a high accumulation in the spleen for the presence of immune cells, and in the liver due to catabolism of the radiotracers. Finally, a correlation between radiotracer uptake in tumors and response to nivolumab treatment has found a higher uptake of both radiotracers in responders: [¹⁸F]BMS-986192 SUV peak (median 6.5 (responder) vs. 3.2 (non-responder), $p = 0.03$), and a similar association was found for [⁸⁹Zr]nivolumab (median SUV peak 6.4 vs. 3.9, $p = 0.019$). Moreover, due to low central nervous system (CNS) tracer penetration, both tracers showed lower accumulation in brain metastases compared to the extracerebral lesions. For non-CNS lesions, the median [¹⁸F]BMS-986192 SUV peak was higher for lesions with $\geq 50\%$ tumor PD-L1 expression by IHC than for lesions with $< 50\%$ expression. Similarly, [⁸⁹Zr]nivolumab uptake was higher in lesions with a higher aggregates of PD-1 positive tumor-infiltrating immune cells at tumor biopsy.

5.1.3. Cytotoxic T-lymphocyte-Associated Protein 4 (CTLA-4) Pathway

The most important studies on CTLA-4 pathways have been conducted by Ehlerding et al. [87,88], which investigated the capacity to visualize CTLA-4 expression in a NSCLC humanized mouse model by in-vivo [⁶⁴Cu]DOTA-ipilimumab, [⁶⁴Cu]NOTA-ipilimumab and [⁶⁴Cu]NOTA-ipilimumab-F(ab')₂ PET images. The visualization of CTLA-4 expression was feasible with all three radiotracers, although all of them demonstrated high absolute uptake in salivary glands, yielding higher salivary gland-to-blood ratios which were slightly lower for F(ab9)₂ (1.78 ± 0.72 vs. 1.19 ± 0.49 , respectively at 48 h). [⁶⁴Cu] labelled ipilimumab (both antibody and fragment) showed a clear salivary gland uptake in humanized mice, and as expected, the fragment showed a faster clearance compared to the entire antibody [87]. Therefore, these radiotracers may help elucidate the response of CTLA-4-targeted checkpoint in immunotherapy, providing a whole-body, in-vivo, non-invasive and quantitative PET imaging of IC biodistribution.

5.1.4. Adoptive Cell Transfer (ACT) Therapy

Different radiotracers for direct and indirect activated cell tracking were developed in the last years [89], such as [⁸⁹Zr]oxine-labelled dendritic cells that showed tumoral uptake at PET imaging of melanoma [90]. Namely, NK cells (designated to eliminate malignant cells [90]) were labelled with an [⁸⁹Zr]oxine complex to perform PET cell tracking in clinically relevant rhesus macaques model for the treatment of hematologic malignancies. Liver, lungs and spleen showed the higher %ID/cc, while a low signal was observed in bone marrow [91]. [⁶⁴Cu]- or [⁸⁹Zr]-labelled antibody against NKp30 were also tested in a renal carcinoma murine model, resulting in an [⁸⁹Zr] higher on-target contrast [92]. Mesenchymal stem cells (MSCs) are multipotent stromal cells that were shown to target tumors, however, their role in neoplastic tissue is still under investigation [93]. To analyze their biodistribution, [¹⁸F]-labelled Fe₃O₄@Al(OH)₃ nanoparticles were used to track MSC after intravenous injection with combined PET/MRI exam, showing intense liver uptake [94].

5.1.5. Chimeric Antigen Receptor T Cell Therapy (CAR-T)

CD8+ cytotoxic T lymphocytes engineered to express both chimeric antigen receptor (IL-13) and herpes simplex virus type-1 thymidine kinase (HSV1-TK) can entrap the PET radiotracer 9-[4-[¹⁸F]fluoro-3-(hydroxymethyl)butyl]guanine [¹⁸F]FHBG within glioma cells. In 2017, Keu et al. [95] showed that non-invasive PET imaging with [¹⁸F]FHBG

can track HSV1-tk reporter gene expression present in CAR-engineered CTLs. In their experience on 7 high-grade gliomas (HGG), [^{18}F]FHBG imaging was safe and enabled the longitudinal imaging of T cells stably transfected with a PET reporter gene in patients. Further, the sodium iodide symporter (NIS) has been proposed as a non-immunogenic radionuclide reporter in ErbB T1E28z CAR therapy in two models of triple-negative breast cancer (MDA-MB-231 and MDA-MB-436). The two models are characterized by a different immune checkpoint inhibitor expression. In particular, MDA-MB-231 has a greater expression of PD-L1 compared to MDA-MB-436, and it is inversely correlated with CAR-T tumor retention [96].

A different strategy involves the direct labelling of IL13R α 2-CAR T cells (as described in the ongoing clinical trial NCT02208362) with [^{89}Zr]oxine in a glioma mouse model delivered intraventricularly or intravenously [51]. The prostate-specific membrane antigen (PSMA) is a human protein and has a low expression in normal tissue. In a study by of Minn et al., anti-CD19 CAR T cells have been transfected to express PSMA, in order to be tracked with [^{18}F]DCFPyL PET in a model of acute lymphoblastic leukemia [97]. UniCAR T cells are modular CAR T cells that can recognize a specific target on the surface of tumor cells. Fused with PSMA-11 epitope, they produce a theragnostic complex that might be useful for retargeting UniCAR T cells in prostate cancer tissue and for treatment response assessment by PET imaging [98].

5.1.6. CD8+ T Lymphocytes

As mentioned above, non-invasive monitoring of active cytotoxic CD8+ T lymphocytes in TME is crucial to predict the immunotherapies' antitumor responses [99,100]. Their presence has been related to a favorable prognosis in different tumors [43,101].

CD8 is expressed on cytotoxic CD8+ T lymphocytes. It is an antigen highly suitable as a target for immune cell-specific radiotracers [102]. A great effort was made in the last years to optimize radiotracers for detection of CD8+ and CD4+ T cells in TME by immuno-PET imaging. One promising approach is a mini-body labeled with [^{89}Zr] that was tested in different immunotherapeutic models, such as colon carcinoma mouse model [102], melanoma, breast, colon, kidney tumor bearing mice [103], gastric adenocarcinoma and HeLa cervical cancer [104]. Of note, the minibody [^{89}Zr]Df-IAB22M2C has been safely tested in human patients affected by different solid malignancies [62]. As expected, the minibody has a fast blood clearance due to its small size, which allows for early image acquisition. A [^{64}Cu]labeled antibody was proposed for the in vivo quantification of CD8+ T cells as a prognostic biomarker in an immunocompetent mouse model of colorectal cancer [105] and breast [106] cancer. Since [^{64}Cu] has a shorter half-life (12.7 h) compared to [^{89}Zr] (78.4 h), the use of [^{64}Cu] reduces patient radiation exposure, thus improving the "acquisition window" compared to shorter-lived PET isotope such as [^{18}F] and [^{68}Ga]. Rashidian et al. demonstrated that a different CD8+ T cell distribution in TME (homogeneous or heterogeneous) can distinguish between responding and non-responding tumors both in melanoma tumor bearing mice treated CTLA-4 therapy [107], and in colorectal adenocarcinoma mouse model treated with anti PD-1 therapy [108]. Namely, in colorectal cancer, both CD8+ and CD11b+ were imaged, and a different distribution was detected in responders and non-responders. A different approach was proposed by Levi et al. using [^{18}F]arabinofuranosyl guanine ([^{18}F]AraG), a substrate for mitochondrial kinase, which is trapped in activated T-cells [109]. Levi et al. compared its performance as immune response radiotracer compared to [^{18}F]FDG in a rhabdomyosarcoma mouse model. Rhabdomyosarcoma, generated by the intramuscular injection of Murine Sarcoma Virus-Moloney Leukemia Virus (MSV-MuLV) is a self-limiting tumor whose rejection, complete by 4 weeks, includes infiltration, activation and proliferation of T cells. As expected, the [^{18}F]FDG signal reflected the glucose consumption showing the maximum uptake when the tumor reached the peak of growth, while [^{18}F]AraG was found to preferentially accumulate in activated CD8+ cells and with a continuous increase during tumor rejection. Of note, in the colon adenocarcinoma mouse model, responders to anti-PD-1 showed a stronger

[¹⁸F]AraG signal before treatment compared to non-responders [110]. The inducible T-cell costimulatory receptor (ICOS), mainly expressed on activated cytotoxic T cells, memory T cells and regulatory T cells, seem more specific than [¹⁸F]FDG and [¹⁸F]AraG [111]. This receptor has been investigated as a PET imaging target for predicting and monitoring T-cell-mediated immune response to cancer immunotherapy. Namely, an [⁸⁹Zr] labeled minibody against ICOS was successfully tested in immunotherapy models of Lewis lung cancer, both in the primary tumor and in tumor-draining lymph nodes. ICOS is an imaging target that allows for an early response detection, before changes in tumor volume occur [112]. In 2017, [¹⁸F] has been directly introduced to the tryptophan backbone, and radioactive 5-¹⁸F-L- α -methyl tryptophan was proposed as indoleamine-2,3-dioxygenase 1 (IDO1) imaging agent. IDO1, preliminary tested on melanoma mice, is responsible for the first step of the degradation of the essential amino acid tryptophan into immunosuppressive kynurenine and its inhibition restores the anti-tumour immune response [113]. In 2020, Pandit-Taskar N et al. [62] assessed the safety and utility of [⁸⁹Zr]IAB22M2C, a radiolabeled minibody against tumor-infiltrating CD8-positive (CD81) T lymphocytes, for targeted imaging of CD81 T cells in cancer patients. This first-in-human prospective study included 6 cancer patients (1 melanoma, 4 lung cancer, and 1 hepatocellular carcinoma). Patients received a single dose of [⁸⁹Zr]IAB22M2C (about 111 MBq), followed by PET/CT scans at different timepoints (until 144 h post administration). No side effects were registered, and serum clearance was biexponential. The highest uptake was observed in the spleen, followed by the bone marrow. The maximum uptake in normal lymph nodes was reached between 24–48 h. Uptake in tumor lesions was seen already 2 h after injection, but the uptake in [⁸⁹Zr]IAB22M2C-positive lesions increased until 24 h (SUV from 5.85 to 22.8).

5.1.7. Other Immuno-PET Radiotracers

Tumor Associated Macrophages (TAM)

Immunosuppressive macrophages in the tumor microenvironment are associated with poor prognosis. A [⁶⁴Cu]-labelled polyglucose nanoparticle (Macrin) was proposed as a radiotracer for quantitative PET imaging of macrophages in colon adenocarcinoma and in orthotopic lung murine tumor models. The diameter of Macrin nanoparticle is 20 nm, and specific macrophage uptake has been demonstrated by dorsal window chambers. The clinical relevance of this nanosystem is in predicting response, especially to TAM-targeted therapies [114]. Integrin CD11 is expressed on the cell surface of TAM that is associated with poor prognosis in high-grade glioma [115]. An [⁸⁹Zr]-labeled anti-CD11b antibody for non-invasive imaging of TAMs showed significant uptake in glioma compared to contralateral normal brain parenchyma [116]. [⁸⁹Zr]HDL has been proposed as tumor macrophagic nanotracer for PET imaging to evaluate the immunotherapeutic response in a mammary adenocarcinoma model [117]. Goggi et al., tested [¹⁸F]FEPPA (N-(2-(2-[¹⁸F]Fluoroethoxy)benzyl)-N-(4-phenoxy-pyridin-3-yl)acetamide, that binds to TSPO), [¹⁸F]FDG and two other radiotracers, [¹⁸F]FB-IL2 and [⁶⁸Ga]mNOTA-GZP (68Ga-NOTA- β -Ala-Gly-Gly-Ile-Glu-Phe-Asp-CHO) that were designed for specific binding of interleukin-2 receptors and granzyme B, respectively. The four radiotracers were directly tested in a murine model of colon cancer, comparing different immunotherapy treatment. While [¹⁸F]FDG, [¹⁸F]FEPPA and [¹⁸F]FB-IL2 were not able to image the immune cell population changes, the [⁶⁸Ga]mNOTA-GZP signal accurately stratified response to combined anti-PD1 and CTLA4 therapy [118].

CD3

CD3 is a direct T-cell marker, and the antibody [⁸⁹Zr]DFO-CD3 was shown to predict xenograft tumor model anti-CTLA-4 therapy response. Three days after [⁸⁹Zr]DFO-CD3 administration, responders showed higher tumor-to-liver PET uptake compared to non-responders [119]. Also, CD3 has been exploited as a T cell marker in BiTE antibody. BiTE stands for “bispecific T-cell engager”. This category represents special antibodies, which are specific for both a surface target antigen on cancer cells and CD3 on T cells. Their

therapeutic efficacy was firstly published in 2009 [120]. Here, an [^{89}Zr]-labelled antibody against CEA and CD3 positive cells showed accumulation in colon and breast tumor in PET, and therapeutic property in CEA positive tumors [121]. The full-sized antibody employed in these applications showed long blood half-life and high liver uptake. However, smaller molecules such as minibodies may have more optimal pharmacokinetic properties. A different possible imaging target expressed on activated T cells is the IL-2 receptor, also called CD25 [122]. The PET radiotracer [^{18}F]FB-IL2 has been described for the first time in 2012 by Di Galleonardo et al. [123]. It showed an enhanced lung tumor uptake after irradiation and/or combination with immunization based on the recombinant Semliki Forest (rSFV) viral-vector [124]. An important challenge on the road to [^{18}F]FB-IL2 clinical translation is its complex and time-consuming production [125]. To overcome this obstacle, the two variants [^{18}F]AIF-RESCA-IL2 and [^{68}Ga]NODAGA-IL2, which are characterized by an easier synthesis, were compared to [^{18}F]FB-IL2. They showed good in-vitro and in-vivo characteristics, with high uptake in lymphoid tissue and human peripheral blood mononuclear cell (hPBMC) xenografts [65].

CD4

CD4+ T cells have also a role in cancer immune response [126]. An anti-CD4 antibody, [^{89}Zr]-labeled GK1.5 cDb [127,128] tested in healthy mice reached a strong %ID/g in inguinal lymph nodes, spleen and kidney.

5.2. [^{18}F]FDG PET/CT

Despite these promising results, the above-mentioned novel radiopharmaceuticals are still all under investigation. In clinical routine, [^{18}F]FDG PET/CT has reached a pivotal role in the evaluation of response to immunotherapy, although it is far from a specific immuno-PET radiotracer. [^{18}F]FDG allows to visualize rapidly proliferating glucose-avid cancer cells (Warburg effect) and monitor immunotherapy response in different cancer types, such as melanoma, non-small-cell lung cancer, head & neck cancer, urothelial cancer and renal cell cancer [129–132]. However, during ICIs therapy, the presence of TILs and the inflammatory response may also lead to a transient increase in tumor volume and increased [^{18}F]FDG uptake in responding tumoral tissue. This phenomenon, known as pseudo-progression, may potentially lead to an underestimation of the benefit of ICIs therapy: Both morphological Response Evaluation Criteria in Solid Tumors (RECIST) 1.1 and functional PET Response Criteria in Solid Tumors version (PERCIST) 1.0 cannot address pseudo-progression adequately [133–135]. Therefore, new morphological and functional criteria have been developed in the last decade to overcome this problem, such as the immune-related response criteria (irRC), the immunotherapy-modified Response Evaluation Criteria in Solid Tumors (imRECIST), the immunotherapy-modified PET Response Criteria in Solid Tumors (imPERCIST), PET Response Evaluation Criteria for Immunotherapy (PERCIMT) and Lymphoma Response to Immunomodulatory Therapy Criteria (LYRIC) [136–140]. The major radiological and functional response criteria to immunotherapy are summarized in Table 3.

Table 3. Summarized the radiological and functional response criteria to the immunotherapy in tumor.

Radiological Response Criteria	irRC	imRECIST
Complete response (CR)	Disappearance of all target lesions. Determined by two observations not less than 4 weeks apart.	Disappearance of all target and non-target lesions, without any new lesions. Any pathological lymph nodes must have reduction in short axis to <10 mm. Determined by two observations not less than 4 weeks apart.
Partial response (PR)	Sum of product of all lesions decreased by >50% for at least 4 weeks; no new lesions; no progression of any lesions.	At least a 30% decrease of the sum of maximum diameters of target lesions; no new lesions; no progression of disease.

Table 3. Cont.

Radiological Response Criteria	irRC	imRECIST	
Stable disease (SD)	Sum of product of all lesions decreased by <50% or increased by <25% in the size of one or more lesions.	Does not meet the criteria for CR, PR or PD, taking as reference the smallest sum of maximum diameters of target lesions.	
Progressive disease (PD)	A single lesion increased by >25% (over the smallest measurement achieved for the single lesion) or the appearance of new lesions, that has to be confirmed in 2 consecutive observations at least 4 weeks apart.	Sum of the maximum diameter of lesions increased by >20% over the smallest achieved sum of maximum diameter. The appearance of new lesions and/or progression of non-target lesions are considered iUPD and must be confirmed 4–8 weeks later as iCPD. Progression is not confirmed in case of shrinkage of these lesions at 4–8 weeks and evaluation must be reset.	
Functional response criteria	imPERCIST	PERCIMT	LYRIC
Complete metabolic response (CMR)	Complete resolution of [¹⁸ F]FDG uptake within all lesions, to a level of less than or equal to that of the mean liver activity and indistinguishable from the background (blood pool uptake).	Complete resolution of [¹⁸ F]FDG uptake within all lesions, to a level of less than or equal to that of the mean liver activity and indistinguishable from the background (blood pool uptake).	PET Deauville score * = 1, 2, or 3, with or without a residual mass on CT, target nodes/nodal masses must regress to <1.5 cm in longest diameter.
Partial metabolic response (PMR)	Reduction of at least 30% in the sum of SULpeak of all target lesions detected at baseline and an absolute drop of 0.8 SULpeak units.	Reduction of at least 30% in the sum of SULpeak of all target lesions detected at baseline and an absolute drop of 0.8 SULpeak units.	PET Deauville score * = 4 or 5 with reduced uptake compared with baseline and residual mass(es) of any size or on CT > 50% decrease in SPD of up to 6 target measurable nodes and extranodal sites.
Stable metabolic disease (SMD)	Does not meet the criteria for CR, PR or PD.	Does not meet the criteria for CR, PR or PD.	Does not meet the criteria for CR, PR or PD.
Progressive metabolic disease (PMD)	Increased of at least 30% in the sum of SULpeak of all target lesions detected at baseline or new FDG-avid lesions are considered UPMD and must be confirmed 4–8 weeks later as CPMD. Progression is not confirmed in case of PMR or SMD at 4–8 weeks and evaluation must be reset.	Progressive disease if: ≥4 new lesions (<1 cm in functional diameter); ≥3 new lesions (>1 cm in functional diameter); ≥2 new lesions (>1.5 cm in functional diameter).	PET Deauville score * = 4 or 5 with an increase in intensity of uptake from baseline and/or new FDG-avid foci consistent with lymphoma at interim or end of-treatment assessment or on CT > 50% increase in SPD of target measurable nodes and extranodal sites. Immune response exception (IR): - IR1 > 50% increase in SPD in first 12 weeks; - IR2 < 50% increase in SPD with new lesion(s) or >50% increase in PPD of a lesion or set of lesions at any time during treatment; - IR3 = increase in FDG uptake without a concomitant increase in lesion size meeting criteria for PD.

Note: CPMD = confirmed progressive metabolic disease; iCPD = immune confirmed progressive disease; imPERCIST = immunotherapy-modified PET Response Criteria in Solid Tumors; imRECIST = immunotherapy-modified Response Evaluation Criteria in Solid Tumors; irRC = immune-related response criteria; iUPD = immune unconfirmed progressive disease; LYRIC = Lymphoma Response to Immunomodulatory Therapy Criteria; PERCIMT = PET Response Evaluation Criteria for Immunotherapy; UPMD = unconfirmed progressive metabolic disease. * Deauville score: 1 = no uptake above background; 2 = uptake < mediastinum; 3 = uptake > mediastinum but < liver; 4 = uptake greater than liver; 5 = uptake markedly higher than liver (2–3 times in normal liver) and/or new lesions; X = new areas of uptake unlikely to be related to lymphoma.

In the morphological criteria, both irRC and imRECIST have introduced the category of immune unconfirmed progressive disease (iUPD) for the appearance of new lesions

at the first restaging, that must be confirmed at least after 4–8 weeks to be reported as immune confirmed progressive disease (iCPD) [141]. In the functional criteria, the indeterminate response, related to the immune-mediated flare effect, has been introduced also in imPERCIST, PERCIMT and LYRIC criteria. Moreover, the complete disappearance of [^{18}F]FDG uptake in all lesions means a complete metabolic response, regardless of a change in tumor size (in contrast to morphological criteria) [142]. Finally, with the intent of differentiating pseudo-progression from true progression, PERCIMT introduced also new criteria of progressive disease (PD), such as the appearance of four or more new lesions (<1.0 cm in functional diameter), or three or more new lesions (>1.0 cm in functional diameter) or two or more new lesions (>1.5 cm in functional diameter) [138]. Compared with morphologic imaging, [^{18}F]FDG PET/CT has also the advantage of an early detection of autoimmune reactions and irAEs (such as hypophysitis, pneumonia, colitis, hepatitis, and thyroiditis) due to increased uptake of [^{18}F]FDG at these sites. This potentially allows for a rapid intervention in life-threatening cases, and aides in switching therapy in less severe cases [142].

In a recent meta-analysis on the incidence of pseudoprogression during ICIs for solid tumor, Park et al. [143] reported that the incidence according to tumor types were similar for the three more representative ones (6.4% in melanoma, 5.0% in NSCLC, and 7.0% in genitourinary cancer). The incidence of pseudoprogression according to the agent types were also analyzed: the pooled incidence in the studies of PD-1/PD-L1 inhibitor monotherapy was 5.7% (5.6% for PD-1 and 6.8% for PD-L1), whereas one study of melanoma that used a CTLA-4 inhibitor showed higher incidence of pseudoprogression (9.7%).

Several semiquantitative parameters, such as metabolic tumor volume (MTV) and total lesion glycolysis (TLG) rate, have been studied to evaluate the predictive and prognostic value of the metabolic tumor burden at baseline [^{18}F]FDG PET/CT. Other parameters, such as spleen to liver ratio (SLR) or bone marrow to liver (BLR) SUVmax ratio, were shown to represent surrogates (indirect index) of the hematopoietic tissue metabolism. Seban et al. [144] in a retrospective study on 55 melanoma patients undergoing 18F-FDG PET/CT before anti-PD1, reported that low tumor burden (TMTV = total metabolic tumor volume; <25 cm³) correlates with survival and objective response, while hematopoietic tissue metabolism (BLR > 0.79; SLR > 0.77) inversely correlates with survival.

These results are considered preliminary but may assume a more prominent role in the evaluation of patients under immunotherapy in the future. Today, the use of [^{18}F]FDG PET/CT is not still standardized in clinical practice and cannot not be considered as a specific marker of immune response.

6. Artificial Intelligence (AI) in Immunotherapy

An improvement in the acquisition, reconstruction and interpretation of medical image datasets is attempted with the use of AI. Through several approaches (Machine learning, radiomics, and deep learning), the dealing with so-called “big-data” is enabled, with the goals to condense information, to enable better patient selection, to improve workflow and to obtain precise predictive models [145].

6.1. Radiomics Assessing the Response to Immunotherapy and Survival Prediction

Radiomic is a new innovative bioinformatic approach to the image’s analysis, that allows to evaluate, through the use of standardized mathematical based models, tumor heterogeneity, quantify predictive and prognostics parameters, radiomic features (RFs), that can be applied in clinical decision support system (CDSS) and in clinical research [146–148]. Radiomics features include first-order statistical functions, which do not detect spatial information (such as conventional, histogram, and shape PET parameters), and second-order and high-order statistical functions, which contain information about the spatial relationships between the intensities of more than two voxels (such as texture parameters). In particular, a better assessment and knowledge of inter- and intra-tumor heterogeneity is essential due to his role in resistance mechanism leading to treatment failure.

Valentinuzzi et al. aimed to investigate whether immunotherapy [^{18}F]FDG radiomics signature (iRADIOMICS) was able to predict response of metastatic NSCLC (stage IV) to pembrolizumab compared to the clinical standards (iRECIST and PD-L1 immunohistochemistry). 30 patients underwent 18F-FDG PET/CT at baseline, and after one and four months. Multivariate iRADIOMICS was found superior to the current standards in terms of predictive power and survival, with an area under the curve (AUC) of 0.90 vs. an AUCmax of 0.6 for PD-L1 and 0.86 for iRECIST [149]. Polverari et al. evaluating evaluated [^{18}F]FDG PET/CT radiomics features extracted from the primary lesion. They were able to predict response to immunotherapy in 57 advanced NSCLC patients. They observed that patients with high tumor volume, tumor lesion glycolysis (TLG), and heterogeneity features (“skewness” and “kurtosis”) had a higher probability of immunotherapy failure [150]. Wei et al. assessed 194 patients with advanced NSCLC through a radiomics signature approach (mpRS) to predict response to immunotherapy using an improved least absolute shrinkage and selection operator (LASSO) method, reaching an AUC of 0.81, with similar results for survival prediction [151]. Park et al. tested radiomics features on pre-gefitinib or pre-erlotinib [^{18}F]FDG PET/CT images, in order to assess their predictive value in recurrence or advanced NSCLC patients with *EGFR* mutation. Radiomics features were found to have an incremental predictive value of early *EGFR* TKI failure, being also highly predictive for PFS assessment [152]. Parvez et al. aimed to determine if [^{18}F]FDG PET/CT radiomics features were able to predict response to immunotherapy and outcome in 82 patients with aggressive B-cell lymphoma. None of the tumor texture features resulted predictive of first-line immunotherapy response, while only a few (i.e., GLNU) correlated with PFS ($p = 0.013$), and OS (kurtosis, $p = 0.035$) [153]. Aide et al. evaluated the prognostic value of [^{18}F]FDG PET/CT radiomics features in 132 diffuse large B-cell lymphoma (DLBCL) patients treated with first-line immune-chemotherapy. The feature Long-Zone High-Grey Level Emphasis (LZHGE) reached the highest receiver operating characteristic (ROC) analysis accuracy (0.76), finally resulting as the only independent predictor of 2y PFS [154]. Pridget et al. recently assessed 29 melanoma patients who underwent [^{18}F]FDG PET/CT at baseline, and at 1, 3, 6 months after immunotherapy, in comparison with seven biological markers and seven clinical variables. They observed that an increase in spleen-to-liver ratio (SLR) greater than 25% at 3 months [^{18}F]FDG PET/CT was associated with poor outcome after immunotherapy [155]. Finally, in a retrospective study on 112 metastatic melanoma patients treated with immune checkpoint inhibition, Basler et al. assessed that a model combined of blood biomarkers (LDH + S100) and non-invasive 18F-FDG PET/CT-based radiomics represent a promising biomarker for early differentiation of pseudo-progression, potentially avoiding added toxicity or delayed treatment switch [156].

6.2. Radiomics Assessing the Molecular Profile

Koyasu et al. developed and evaluated a radiomics approach for classifying histological subtypes and *EGFR* mutational status in 156 adenocarcinomas and 32 squamous cell carcinomas based on [^{18}F]FDG PET/CT images. Authors used two different machine-learning algorithms (random forest and gradient tree boosting-XGB). For the classification of histological subtypes and *EGFR* mutation status, the highest AUC was obtained with XGB in the multiple types analysis (0.843 and 0.659, respectively) [157]. Zhang et al. assessed the predictive value of pre-immunotherapy [^{18}F]FDG PET/CT-based radiomics features for *EGFR* mutational status in 248 NSCLC. Their radiomics model (10 features) was able to discriminate between *EGFR* mutation and *EGFR* wild-type, with an AUCmax of 0.75 for the clinical model, increasing to 0.87 in combination with clinical variables [158]. Also Li et al. aimed to demonstrate the connection between mutations and phenotypes in 115 NSCLC, using somatic mutation testing and [^{18}F]FDG PET/CT image analysis. A radiomics signature based on both PET and CT radiomics features outperformed individual radiomics features and the conventional PET parameters in discriminating between mutant and wild-type *EGFR* (AUC of 0.805) [159]. Further, the group of Jiang et al. investigated whether quantitative and qualitative [^{18}F]FDG PET/CT features can be used as imaging

biomarkers for the *EGFR* mutational status in 80 NSCLC. The 35 selected features were significantly associated with *EGFR* mutational status, and the built predictive model reached an AUC of 0.953 [160]. Jiang et al. explored the potential value of radiomics features from [¹⁸F]PET/CT in assessing different PD-L1 mutational status in 399 NSCLC. For the prediction of a PD-L1 (Sp142) expression level >1%, a model based on CT features yielded an AUC of 0.97, and AUC 0.97 for [¹⁸F]FDG PET/CT, as well. For the prediction of PD-L1 (Sp142) expression level >50%, [¹⁸F]FDG PET/CT features model resulted in an AUC of 0.77 and AUC 0.8 for CT features. [161].

6.3. Deep-Learning Approach

Deep-learning (DL) is an AI application organized in multiple, progressive neural networks and subsequent related processes (layers). DL approaches simultaneously learn relevant features and prediction models from input images with no need of previous computation and extraction of “custom-tailored” imaging variables. Park et al. developed a DL model to predict cytolytic activity score (CytAct), using semi-automatically segmented tumors on [¹⁸F]FDG PET/CT paired with tissue RNA sequencing. In the immune checkpoint blockade (ICB) cohort, a higher predicted CytAct of an individual lesion was associated with more tumor shrinkage after ICB treatment ($p < 0.001$). Furthermore, higher minimum predicted CytAct in each patient was associated with significantly prolonged PFS and OS ($p = 0.001$ and $p = 0.004$, respectively), while in patients with multiple lesions, ICB responders had significantly lower variance of predicted CytActs ($p = 0.005$) [162].

7. Discussion

As aforementioned, the selection and the response to immunotherapy is based on several mechanisms that play different roles. ICs expression on tumor cells seems to be a necessary, but not sufficient information to prove sufficient insights into immune mechanisms related to immunotherapy efficacy, to select patients candidate to immunotherapy and to predict the response to treatment [43,44].

In 2018, Kather et al. [163] introduced the concept of spatial immune infiltration patterns (‘topography’) across cancer entities and across various immune cell types, studying 965 histological tissue slides from 177 patients in a pan-cancer cohort. They showed how a bivariate classification system based on this ‘topography’ can stratify patients and can be considered as a biomarker for patients with solid tumors and candidate to immunotherapy. In a recent review, Pietrobon et al. [164] listed the three distinct “immune topographies”: *hot tumors* characterized by lymphocytes infiltration, mixed with tumor cells in the tumor core; *cold tumors*, characterized by an absence of lymphocytes infiltrations (i.e., almost no lymphocytes can be seen on histological slides); and *immune-excluded tumors* characterized by an abundance of lymphocytes at the invasive edge of the tumor, but few to no lymphocytes in the tumor core. This third type of tumor display gradients of T-cell exclusion, specific to each tumor environment and not present in *cold tumors*, where T cells are completely absent.

ImmunoPET radiotracer, ICO PET radiotracer and [¹⁸F]FDG give the possibility to systematically mapping these “immune topographies” in both spatial and temporal distribution: - stratifying patient at baseline, before starting a systemic treatment such as immunotherapy or chemotherapy; - providing also important quantitative information, based on conventional and radiomic PET parameters and on dynamic acquisition, that can help to adjust treatment accordingly to immunoPET expression; monitoring “immune topographies” changes during immunotherapies, through the evaluation of delta-changed of conventional and radiomic PET parameters, helping an early change of therapy in non-responder patients or in case of toxicity.

In-vivo molecular imaging of ICs expression, especially with the use of combined radiotracers, which provide different informations, may be more predictive than in-vitro analysis of TME. In-vivo molecular imaging provide also the added value of a whole-body evaluation and not limited to a single anatomical sample, leading to the evaluation of the

tumor heterogeneity and to the identification of potential non-responding lesions, which need different and/or combined treatment in a personalized medicine approach.

ImmunoPET radiotracers could be moreover useful to detect early signs of drug resistance and to distinguish tumor progression from pseudo-progression, especially if combined with [^{18}F]FDG PET/CT images. Moreover, in this contest, ICOS PET radiotracers may have an added value to predict early response to therapy: reasonably, the physician should change therapies regime (switching or combining with other therapies) to the patients, in which ICOS PET shows low or no uptake of activate T cells.

Both immunoPET and ICOS PET seems extremely promising improving clinical patient management, even if ICOS PET seems more versatile than immunoPET and in both cases presumably the information obtained from these radiotracers will still have to be integrated with that extracted from the [^{18}F]FDG PET/CT images.

Certainly, functional imaging with PET/CT does not allow analysis of these phenomena at the microscopic level, and biopsy and tissue analysis is still mandatory and strictly necessary. However, immunoPET, ICO and [^{18}F]FDG PET/CT images can better guide biopsy for both baseline assessment and restaging in case of disease progression. Combining both the micro- and macroscopic informations, it will be possible to obtain faster a higher level of knowledge about tumor and TME behavior.

8. Conclusions

In recent decades, the impressive improvement in translational medicine has led to a better understanding of the TME and all the dynamic mechanisms behind tumor development and growth, such as the relationship between tumor cells and infiltrating immune cells in the TME. These discoveries have led to the development of immunotherapy, and subsequently of imaging biomarkers for the TME, which may provide new insights into TME and cancer behavior. While most of these new radiotracers are still in a preclinical phase, they will certainly provide complementary information to clinically used [^{18}F]FDG PET/CT for the prediction of immunotherapy response in the context of personalized medicine, also broadening the theragnostic horizon. Today, [^{18}F]FDG PET/CT represent a standard technique employed for tumor staging and response assessment, despite the known limitations due to pseudo progression and enhanced activity of inflammatory components. Therefore, [^{18}F]FDG PET/CT is still not validated as a specific biomarker in immunotherapy and not well established for response assessment, yet. Nevertheless, new developments in PET/CT technology and images analysis are becoming fundamental tools to guide therapeutic decision-making and prognosis stratification in clinical practice. AI-based approaches may help identify subpopulations with an increased risk of immunotherapy failure, assessing the immune-profile non-invasively, and predicting survival. Hence, they may well evolve as a fundamental support for clinical decision-making. However, due to problems related to data standardization, privacy concerns, lack of extensive data, the development of AI approaches is still challenging. In our opinion and according to the presented data, new radiotracers combined with technical improvements and AI applications will further refine the selection of the most appropriate therapy for each patient, thus potentially avoiding high-cost strategies (not exempt from toxicity), towards individualized precision healthcare.

Author Contributions: Substantial contributions to the conception or design of the work: D.D.; Literature search: V.L., R.L. and M.C.; Article selection: V.L., R.L. and M.C.; Manuscript preparation: V.L., R.L. and M.C.; Drafting the work or revising it critically for important intellectual content: all authors. All authors have read and agreed to the published version of the manuscript.

Funding: This research received no external funding.

Institutional Review Board Statement: Not applicable.

Informed Consent Statement: Not applicable.

Acknowledgments: Figures 1 and 2 have been created with BioRender.com. These images had been adapted from: (1) “Pro- and Anti-Tumour Immune Cells in the Tumor Microenvironment”, by BioRender.com (2021). Retrieved from <https://app.biorender.com/biorender-templates/t-5fc930de9e43ce3283cc6197-pro-and-anti-tumour-immune-cells-in-the-tumor-microenvironme> (1 March 2021); (2) “Tumor Microenvironment 2”, by BioRender.com (2021). Retrieved from <https://app.biorender.com/biorender-templates/t-5f63a4bebecfd300b1f68c0c-tumor-microenvironment-2> (1 March 2021); (3) “Overview of Metastatic Cascade”, by BioRender.com (2021). Retrieved from <https://app.biorender.com/biorender-templates/t-5f46e7082c321c00b3f65e38-overview-of-metastatic-cascade> (1 March 2021); (4) “Immunotherapy Overview”, by BioRender.com (2021). Retrieved from <https://app.biorender.com/biorender-templates/t-5f2da5b6a2391a00a70941ba-immunotherapy-overview> (1 March 2021); (5) “T-cell Deactivation vs. Activation”, by BioRender.com (2021). Retrieved from <https://app.biorender.com/biorender-templates/t-5c082704e97e1400127428b8-t-cell-deactivation-vs-activation>; (6) “CAR T Cell Therapy Overview”, by BioRender.com (2021). Retrieved from <https://app.biorender.com/biorender-templates/t-5e41ad5c0dd2690088b718bd-car-t-cell-therapy-overview> (1 March 2021).

Conflicts of Interest: MH is a recipient of grants from GE Healthcare, grants for translational and clinical cardiac and oncological research from the Alfred and Annemarie von Sick Grant legacy, and grants from the Artificial Intelligence in oncological Imaging Network by the University of Zurich. IAB is a recipient of grants from GE Healthcare, grants from the Sick legacy and the “Jimmy Wirth Foundation”. The other authors declare no conflict of interest.

Abbreviations

[⁶⁴Cu] = copper-64; [⁸⁹Zr] = zirconium-89; %ID/cc = percent injected dose per cubic centimeter in tissue; ACT = adoptive cell transfer; CR = complete response; CT = computer tomography; CTLA-4 = cytotoxic T-lymphocyte-associated protein 4; DFO = deferoxamine; EGFR = epidermal growth factor receptor; EMA = European Medicines Agency; FDA = Food and Drug Administration; [¹⁸F]FDG = 2-deoxy-2-[¹⁸F]fluoro-D-glucose; ICIs = immune checkpoint inhibitors; IHC = immunohistochemistry; IL2 = interleukin-2; irAE = immune-related adverse event; mAb = monoclonal antibody; MHC-I or -II = major histocompatibility complex-I or -II; MR = magnetic resonance; OS = overall survival; OTR = objective tumor response; PD = progressive disease; PD-1 = programmed cell death protein 1; PD-L1 = programmed cell death ligand 1; PD-L2 = programmed cell death ligand 2; PERCIST = positron emission tomography response criteria in solid tumors; PET = positron emission tomography; PFS = progression free survival; PR = partial response; RECIST = response evaluation criteria in solid tumors; SD = stable disease; SPECT = single-photon emission computed tomography; SUV = standardized uptake value; TAM = tumor associated macrophage; TGF-β = transforming growth factor beta; TKI = tyrosine kinase inhibitors; TME = tumor microenvironment; Tregs = regulatory T cells.

References

1. Zhang, Y.; Zhang, Z. The history and advances in cancer immunotherapy: Understanding the characteristics of tumor-infiltrating immune cells and their therapeutic implications. *Cell. Mol. Immunol.* **2020**, *17*, 807–821. [[CrossRef](#)]
2. Liberati, A.; Altman, D.G.; Tetzlaff, J.; Mulrow, C.; Gøtzsche, P.C.; Ioannidis, J.P.A.; Clarke, M.; Devereaux, P.J.; Kleijnen, J.; Moher, D. The PRISMA statement for reporting systematic reviews and meta-analyses of studies that evaluate health care interventions: Explanation and elaboration. *J. Clin. Epidemiol.* **2009**, *62*, e1–e34. [[CrossRef](#)] [[PubMed](#)]
3. Galli, F.; Aguilera, J.V.; Palermo, B.; Markovic, S.N.; Nisticò, P.; Signore, A. Relevance of immune cell and tumor microenvironment imaging in the new era of immunotherapy. *J. Exp. Clin. Cancer Res.* **2020**, *39*, 1–21. [[CrossRef](#)] [[PubMed](#)]
4. Janco, J.M.T.; Lamichhane, P.; Karyampudi, L.; Knutson, K.L. Tumor-Infiltrating Dendritic Cells in Cancer Pathogenesis. *J. Immunol.* **2015**, *194*, 2985–2991. [[CrossRef](#)]
5. Gonzalez, H.; Hagerling, C.; Werb, Z. Roles of the immune system in cancer: From tumor initiation to metastatic progression. *Genes Dev.* **2018**, *32*, 1267–1284. [[CrossRef](#)] [[PubMed](#)]
6. Josefowicz, S.Z.; Lu, L.F.; Rudensky, A.Y. Regulatory T Cells: Mechanisms of Differentiation and Function. *Annu. Rev. Immunol.* **2012**, *30*, 531–564. [[CrossRef](#)] [[PubMed](#)]
7. Mantovani, A.; Marchesi, F.; Malesci, A.; Laghi, L.; Allavena, P. Tumour-associated macrophages as treatment targets in oncology. *Nat. Rev. Clin. Oncol.* **2017**, *14*, 399–416. [[CrossRef](#)]
8. Mantovani, A.; Sozzani, S.; Locati, M.; Allavena, P.; Sica, A. Macrophage polarization: Tumor-associated macrophages as a paradigm for polarized M2 mononuclear phagocytes. *Trends Immunol.* **2002**, *23*, 549–555. [[CrossRef](#)]

9. Lecot, P.; Sarabi, M.; Abrantes, M.P.; Mussard, J.; Koenderman, L.; Caux, C.; Bendriss-Vermare, N.; Michallet, M.-C. Neutrophil Heterogeneity in Cancer: From Biology to Therapies. *Front. Immunol.* **2019**, *10*, 2155. [[CrossRef](#)]
10. Nielsen, J.S.; Sahota, R.A.; Milne, K.; Kost, S.E.; Nesslinger, N.J.; Watson, P.H.; Nelson, B.H. CD20+ Tumor-Infiltrating Lymphocytes Have an Atypical CD27– Memory Phenotype and Together with CD8+ T Cells Promote Favorable Prognosis in Ovarian Cancer. *Clin. Cancer Res.* **2012**, *18*, 3281–3292. [[CrossRef](#)]
11. Al-Shibli, K.I.; Donnem, T.; Al-Saad, S.; Persson, M.; Bremnes, R.M.; Busund, L.-T. Prognostic Effect of Epithelial and Stromal Lymphocyte Infiltration in Non–Small Cell Lung Cancer. *Clin. Cancer Res.* **2008**, *14*, 5220–5227. [[CrossRef](#)]
12. Cabrita, R.; Lauss, M.; Sanna, A.; Donia, M.; Larsen, M.S.; Mitra, S.; Johansson, I.; Phung, B.; Harbst, K.; Vallon-Christersson, J.; et al. Tertiary lymphoid structures improve immunotherapy and survival in melanoma. *Nature* **2020**, *577*, 561–565. [[CrossRef](#)]
13. Shalpour, S.; Font-Burgada, J.; Di Caro, G.; Zhong, Z.; Sanchez-Lopez, E.; Dhar, D.; Willimsky, G.; Ammirante, M.; Strasner, A.; Hansel, D.E.; et al. Immunosuppressive plasma cells impede T-cell-dependent immunogenic chemotherapy. *Nature* **2015**, *521*, 94–98. [[CrossRef](#)]
14. Waldman, A.D.; Fritz, J.M.; Lenardo, M.J. A guide to cancer immunotherapy: From T cell basic science to clinical practice. *Nat. Rev. Immunol.* **2020**, *20*, 651–668. [[CrossRef](#)] [[PubMed](#)]
15. Bouleau, A.; Lebon, V.; Truillet, C. PET imaging of immune checkpoint proteins in oncology. *Pharmacol. Ther.* **2021**, *222*, 107786. [[CrossRef](#)] [[PubMed](#)]
16. Sun, C.; Mezzadra, R.; Schumacher, T.N. Regulation and Function of the PD-L1 Checkpoint. *Immunity* **2018**, *48*, 434–452. [[CrossRef](#)]
17. Rowshanravan, B.; Halliday, N.; Sansom, D.M. CTLA-4: A moving target in immunotherapy. *Blood* **2018**, *131*, 58–67. [[CrossRef](#)] [[PubMed](#)]
18. Pardoll, D.M. The blockade of immune checkpoints in cancer immunotherapy. *Nat. Rev. Cancer* **2012**, *12*, 252–264. [[CrossRef](#)]
19. Martinez, M.; Moon, E.K. CAR T Cells for Solid Tumors: New Strategies for Finding, Infiltrating, and Surviving in the Tumor Microenvironment. *Front. Immunol.* **2019**, *10*, 128. [[CrossRef](#)]
20. Muhammad, N.; Mao, Q.; Xia, H. CAR T-cells for cancer therapy. *Biotechnol. Genet. Eng. Rev.* **2017**, *33*, 190–226. [[CrossRef](#)]
21. Marofi, F.; Motavalli, R.; Safonov, V.A.; Thangavelu, L.; Yumashev, A.V.; Alexander, M.; Shomali, N.; Chartrand, M.S.; Pathak, Y.; Jarahian, M.; et al. CAR T cells in solid tumors: Challenges and opportunities. *Stem Cell Res. Ther.* **2021**, *12*, 8. [[CrossRef](#)] [[PubMed](#)]
22. Porter, D.L.; Levine, B.L.; Kalos, M.; Bagg, A.; June, C.H. Chimeric Antigen Receptor–Modified T Cells in Chronic Lymphoid Leukemia. *N. Engl. J. Med.* **2011**, *365*, 725–733. [[CrossRef](#)]
23. Chimeric Antigen Receptor–Modified T Cells in Chronic Lymphoid Leukemia; Chimeric Antigen Receptor–Modified T Cells for Acute Lymphoid Leukemia; Chimeric Antigen Receptor T Cells for Sustained Remissions in Leukemia. *N. Engl. J. Med.* **2016**, *374*, 998. [[CrossRef](#)] [[PubMed](#)]
24. Brentjens, R.J.; Davila, M.L.; Riviere, I.; Park, J.; Wang, X.; Cowell, L.G.; Bartido, S.; Stefanski, J.; Taylor, C.; Olszewska, M.; et al. CD19-Targeted T Cells Rapidly Induce Molecular Remissions in Adults with Chemotherapy-Refractory Acute Lymphoblastic Leukemia. *Sci. Transl. Med.* **2013**, *5*, 177ra38. [[CrossRef](#)] [[PubMed](#)]
25. Andtbacka, R.H.I.; Kaufman, H.L.; Collichio, F.; Amatruda, T.; Senzer, N.; Chesney, J.; Delman, K.A.; Spitler, L.E.; Puzanov, I.; Agarwala, S.S.; et al. Talimogene Laherparepvec Improves Durable Response Rate in Patients with Advanced Melanoma. *J. Clin. Oncol.* **2015**, *33*, 2780–2788. [[CrossRef](#)]
26. Killock, D. Skin cancer: T-VEC oncolytic viral therapy shows promise in melanoma. *Nat. Rev. Clin. Oncol.* **2015**, *12*, 438. [[CrossRef](#)]
27. Kawakami, Y.; Eliyahu, S.; Delgado, C.H.; Robbins, P.F.; Sakaguchi, K.; Appella, E.; Yannelli, J.R.; Adema, G.J.; Miki, T.; Rosenberg, S.A. Identification of a human melanoma antigen recognized by tumor-infiltrating lymphocytes associated with in vivo tumor rejection. *Proc. Natl. Acad. Sci. USA* **1994**, *91*, 6458–6462. [[CrossRef](#)]
28. Jandus, C.; Bioley, G.; Dojcinovic, D.; Derré, L.; Baitsch, L.; Wieckowski, S.; Rufer, N.; Kwok, W.W.; Tiercy, J.-M.; Luescher, I.F.; et al. Tumor Antigen–Specific FOXP3+ CD4 T Cells Identified in Human Metastatic Melanoma: Peptide Vaccination Results in Selective Expansion of Th1-like Counterparts. *Cancer Res.* **2009**, *69*, 8085–8093. [[CrossRef](#)] [[PubMed](#)]
29. Van Der Bruggen, P.; Traversari, C.; Chomez, P.; Lurquin, C.; De Plaen, E.; Eynde, B.V.D.; Knuth, A.; Boon, T. A gene encoding an antigen recognized by cytolytic T lymphocytes on a human melanoma. *Science* **1991**, *254*, 1643–1647. [[CrossRef](#)]
30. Kantoff, P.W.; Higano, C.S.; Shore, N.D.; Berger, E.R.; Small, E.J.; Penson, D.F.; Redfern, C.H.; Ferrari, A.C.; Dreicer, R.; Sims, R.B.; et al. Sipuleucel-T Immunotherapy for Castration-Resistant Prostate Cancer. *N. Engl. J. Med.* **2010**, *363*, 411–422. [[CrossRef](#)]
31. Hodi, F.S.; O’Day, S.J.; McDermott, D.F.; Weber, R.W.; Sosman, J.A.; Haanen, J.B.; Gonzalez, R.; Robert, C.; Schadendorf, D.; Hassel, J.C.; et al. Improved Survival with Ipilimumab in Patients with Metastatic Melanoma. *N. Engl. J. Med.* **2010**, *363*, 711–723. [[CrossRef](#)]
32. Vaddepally, R.K.; Kharel, P.; Pandey, R.; Garje, R.; Chandra, A.B. Review of Indications of FDA-Approved Immune Checkpoint Inhibitors per NCCN Guidelines with the Level of Evidence. *Cancers* **2020**, *12*, 738. [[CrossRef](#)] [[PubMed](#)]
33. Larimer, B.M.; Wehrenberg-Klee, E.; Dubois, F.; Mehta, A.; Kalomeris, T.; Flaherty, K.; Boland, G.; Mahmood, U. Granzyme B PET Imaging as a Predictive Biomarker of Immunotherapy Response. *Cancer Res.* **2017**, *77*, 2318–2327. [[CrossRef](#)] [[PubMed](#)]
34. Luke, J.J.; Flaherty, K.T.; Ribas, A.; Long, G.V. Targeted agents and immunotherapies: Optimizing outcomes in melanoma. *Nat. Rev. Clin. Oncol.* **2017**, *14*, 463–482. [[CrossRef](#)]
35. Hamid, O.; Robert, C.; Daud, A.; Hodi, F.S.; Hwu, W.-J.; Kefford, R.; Wolchok, J.D.; Hersey, P.; Joseph, R.W.; Weber, J.S.; et al. Safety and Tumor Responses with Lambrolizumab (Anti-PD-1) in Melanoma. *N. Engl. J. Med.* **2013**, *369*, 134–144. [[CrossRef](#)]

36. Topalian, S.L.; Hodi, F.S.; Brahmer, J.R.; Gettinger, S.N.; Smith, D.C.; McDermott, D.F.; Powderly, J.D.; Carvajal, R.D.; Sosman, J.A.; Atkins, M.B.; et al. Safety, Activity, and Immune Correlates of Anti-PD-1 Antibody in Cancer. *N. Engl. J. Med.* **2012**, *366*, 2443–2454. [[CrossRef](#)]
37. Kluger, H.M.; Zito, C.R.; Turcu, G.; Baine, M.K.; Zhang, H.; Adeniran, A.; Sznol, M.; Rimm, D.L.; Kluger, Y.; Chen, L.; et al. PD-L1 Studies Across Tumor Types, Its Differential Expression and Predictive Value in Patients Treated with Immune Checkpoint Inhibitors. *Clin. Cancer Res.* **2017**, *23*, 4270–4279. [[CrossRef](#)]
38. Tunger, A.; Sommer, U.; Wehner, R.; Kubasch, A.S.; Grimm, M.-O.; Bachmann, M.P.; Platzbecker, U.; Bornhäuser, M.; Baretton, G.; Schmitz, M. The Evolving Landscape of Biomarkers for Anti-PD-1 or Anti-PD-L1 Therapy. *J. Clin. Med.* **2019**, *8*, 1534. [[CrossRef](#)] [[PubMed](#)]
39. Mastracci, L.; Fontana, V.; Queirolo, P.; Carosio, R.; Grillo, F.; Morabito, A.; Banelli, B.; Tanda, E.; Boutros, A.; Dozin, B.; et al. Response to ipilimumab therapy in metastatic melanoma patients: Potential relevance of CTLA-4+ tumor infiltrating lymphocytes and their in situ localization. *Cancer Immunol. Immunother.* **2020**, *69*, 653–662. [[CrossRef](#)]
40. Gerlinger, M.; Rowan, A.J.; Horswell, S.; Larkin, J.; Endesfelder, D.; Gronroos, E.; Martinez, P.; Matthews, N.; Stewart, A.; Tarpey, P.; et al. Intratumor Heterogeneity and Branched Evolution Revealed by Multiregion Sequencing. *N. Engl. J. Med.* **2012**, *366*, 883–892. [[CrossRef](#)] [[PubMed](#)]
41. Ziv, E.; Durack, J.C.; Solomon, S.B. The Importance of Biopsy in the Era of Molecular Medicine. *Cancer J.* **2016**, *22*, 418–422. [[CrossRef](#)]
42. McQuerry, J.A.; Chang, J.T.; Bowtell, D.D.L.; Cohen, A.; Bild, A.H. Mechanisms and clinical implications of tumor heterogeneity and convergence on recurrent phenotypes. *J. Mol. Med.* **2017**, *95*, 1167–1178. [[CrossRef](#)]
43. Fridman, W.H.; Zitvogel, L.; Sautès-Fridman, C.; Kroemer, G. The immune contexture in cancer prognosis and treatment. *Nat. Rev. Clin. Oncol.* **2017**, *14*, 717–734. [[CrossRef](#)]
44. Zou, Y.; Hu, X.; Zheng, S.; Yang, A.; Li, X.; Tang, H.; Kong, Y.; Xie, X. Discordance of immunotherapy response predictive biomarkers between primary lesions and paired metastases in tumours: A multidimensional analysis. *EBioMedicine* **2021**, *63*, 103137. [[CrossRef](#)]
45. De Jong, M.; Essers, J.; Van Weerden, W.M. Imaging preclinical tumour models: Improving translational power. *Nat. Rev. Cancer* **2014**, *14*, 481–493. [[CrossRef](#)]
46. Graham, M.M. Clinical Molecular Imaging with Radiotracers: Current Status. *Med. Princ. Pract.* **2012**, *21*, 197–208. [[CrossRef](#)]
47. Sharma, R.; Aboagye, E. Development of radiotracers for oncology—the interface with pharmacology. *Br. J. Pharmacol.* **2011**, *163*, 1565–1585. [[CrossRef](#)]
48. Abousaway, O.; Rakhshandehroo, T.; Abbeele, A.D.V.D.; Kircher, M.F.; Rashidian, M. Noninvasive Imaging of Cancer Immunotherapy. *Nanotheranostics* **2021**, *5*, 90–112. [[CrossRef](#)] [[PubMed](#)]
49. Meidenbauer, N.; Marienhagen, J.; Laumer, M.; Vogl, S.; Heymann, J.; Andreesen, R.; Mackensen, A. Survival and tumor localization of adoptively transferred Melan-A-specific T cells in melanoma patients. *J. Immunol.* **2003**, *170*, 2161–2169. [[CrossRef](#)] [[PubMed](#)]
50. Bansal, A.; Pandey, M.K.; Demirhan, Y.E.; Nesbitt, J.J.; Crespo-Diaz, R.J.; Terzic, A.; Behfar, A.; DeGrado, T.R. Novel ⁸⁹Zr cell labeling approach for PET-based cell trafficking studies. *EJNMMI Res.* **2015**, *5*, 19. [[CrossRef](#)] [[PubMed](#)]
51. Weist, M.R.; Starr, R.; Aguilar, B.; Chea, J.; Miles, J.K.; Poku, E.; Gerdts, E.; Yang, X.; Priceman, S.J.; Forman, S.J.; et al. PET of Adoptively Transferred Chimeric Antigen Receptor T Cells with ⁸⁹Zr-Oxine. *J. Nucl. Med.* **2018**, *59*, 1531–1537. [[CrossRef](#)] [[PubMed](#)]
52. Kurebayashi, Y.; Choyke, P.L.; Sato, N. Imaging of cell-based therapy using ⁸⁹Zr-oxine ex vivo cell labeling for positron emission tomography. *Nanotheranostics* **2021**, *5*, 27–35. [[CrossRef](#)]
53. Severin, G.W.; Engle, J.W.; Barnhart, T.E.; Nickles, R.J. ⁸⁹Zr Radiochemistry for Positron Emission Tomography. *Med. Chem.* **2011**, *7*, 389–394. [[CrossRef](#)]
54. McCarthy, C.E.; White, J.M.; Viola, N.T.; Gibson, H.M. In vivo Imaging Technologies to Monitor the Immune System. *Front. Immunol.* **2020**, *11*, 1067. [[CrossRef](#)]
55. Xenaki, K.T.; Oliveira, S.; Henegouwen, P.M.P.V.B.E. Antibody or Antibody Fragments: Implications for Molecular Imaging and Targeted Therapy of Solid Tumors. *Front. Immunol.* **2017**, *8*, 1287. [[CrossRef](#)]
56. Thurber, G.M.; Zajic, S.C.; Wittrup, K.D. Theoretic Criteria for Antibody Penetration into Solid Tumors and Micrometastases. *J. Nucl. Med.* **2007**, *48*, 995–999. [[CrossRef](#)]
57. Thurber, G.M.; Schmidt, M.M.; Wittrup, K.D. Antibody tumor penetration: Transport opposed by systemic and antigen-mediated clearance. *Adv. Drug Deliv. Rev.* **2008**, *60*, 1421–1434. [[CrossRef](#)]
58. Yu, S.; Li, A.; Liu, Q.; Yuan, X.; Xu, H.; Jiao, D.; Pestell, R.G.; Han, X.; Wu, K. Recent advances of bispecific antibodies in solid tumors. *J. Hematol. Oncol.* **2017**, *10*, 1–16. [[CrossRef](#)]
59. Chatterjee, S.; Lesniak, W.G.; Miller, M.S.; Lisok, A.; Sikorska, E.; Wharram, B.; Kumar, D.; Gabrielson, M.; Pomper, M.G.; Gabelli, S.B.; et al. Rapid PD-L1 detection in tumors with PET using a highly specific peptide. *Biochem. Biophys. Res. Commun.* **2017**, *483*, 258–263. [[CrossRef](#)] [[PubMed](#)]
60. Niemeijer, A.N.; Leung, D.; Huisman, M.C.; Bahce, I.; Hoekstra, O.S.; Van Dongen, G.A.M.S.; Boellaard, R.; Du, S.; Hayes, W.; Smith, R.; et al. Whole body PD-1 and PD-L1 positron emission tomography in patients with non-small-cell lung cancer. *Nat. Commun.* **2018**, *9*, 1–5. [[CrossRef](#)] [[PubMed](#)]

61. Bensch, F.; Van Der Veen, E.L.; Lub-de Hooge, M.N.; Jorritsma-Smit, A.; Boellaard, R.; Kok, I.C.; Oosting, S.F.; Schröder, C.P.; Hiltermann, T.J.N.; Van Der Wekken, A.J.; et al. ⁸⁹Zr-atezolizumab imaging as a non-invasive approach to assess clinical response to PD-L1 blockade in cancer. *Nat. Med.* **2018**, *24*, 1852–1858. [[CrossRef](#)]
62. Pandit-Taskar, N.; Postow, M.A.; Hellmann, M.D.; Harding, J.J.; Barker, C.A.; O'Donoghue, J.A.; Ziolkowska, M.; Ruan, S.; Lyashchenko, S.K.; Tsai, F.; et al. First-in-Humans Imaging with ⁸⁹Zr-Df-IAB22M2C Anti-CD8 Minibody in Patients with Solid Malignancies: Preliminary Pharmacokinetics, Biodistribution, and Lesion Targeting. *J. Nucl. Med.* **2020**, *61*, 512–519. [[CrossRef](#)] [[PubMed](#)]
63. Natarajan, A.; Mayer, A.T.; Xu, L.; Reeves, R.E.; Gano, J.; Gambhir, S.S. Novel Radiotracer for ImmunoPET Imaging of PD-1 Checkpoint Expression on Tumor Infiltrating Lymphocytes. *Bioconjug. Chem.* **2015**, *26*, 2062–2069. [[CrossRef](#)] [[PubMed](#)]
64. Josefsson, A.; Nedrow, J.R.; Park, S.; Banerjee, S.R.; Rittenbach, A.; Jammes, F.; Tsui, B.; Sgouros, G. Imaging, Biodistribution, and Dosimetry of Radionuclide-Labeled PD-L1 Antibody in an Immunocompetent Mouse Model of Breast Cancer. *Cancer Res.* **2016**, *76*, 472–479. [[CrossRef](#)] [[PubMed](#)]
65. Van Der Veen, E.L.; Suurs, F.V.; Cleeren, F.; Bormans, G.; Elsinga, P.H.; Hospers, G.A.P.; Hooge, M.N.L.-D.; De Vries, E.G.E.; De Vries, E.F.J.; Antunes, I.F. Development and Evaluation of Interleukin-2-Derived Radiotracers for PET Imaging of T Cells in Mice. *J. Nucl. Med.* **2020**, *61*, 1355–1360. [[CrossRef](#)]
66. Li, M.; Ehlerding, E.B.; Jiang, D.; E Barnhart, T.; Chen, W.; Cao, T.; Engle, J.W.; Cai, W. In vivo characterization of PD-L1 expression in breast cancer by immuno-PET with ⁸⁹Zr-labeled avelumab. *Am. J. Transl. Res.* **2020**, *12*, 1862–1872.
67. Kumar, D.; Lisok, A.; Dahmane, E.; McCoy, M.; Shelake, S.; Chatterjee, S.; Allaj, V.; Sysa-Shah, P.; Wharram, B.; Lesniak, W.G.; et al. Peptide-based PET quantifies target engagement of PD-L1 therapeutics. *J. Clin. Investig.* **2019**, *129*, 616–630. [[CrossRef](#)]
68. Bao, R.; Wang, Y.; Lai, J.; Zhu, H.; Zhao, Y.; Li, S.; Li, N.; Huang, J.; Yang, Z.; Wang, F.; et al. Enhancing Anti-PD-1/PD-L1 Immune Checkpoint Inhibitory Cancer Therapy by CD276-Targeted Photodynamic Ablation of Tumor Cells and Tumor Vasculature. *Mol. Pharm.* **2019**, *16*, 339–348. [[CrossRef](#)]
69. Kikuchi, M.; Clump, D.A.; Srivastava, R.M.; Sun, L.; Zeng, D.; Diaz-Perez, J.A.; Anderson, C.J.; Edwards, W.B.; Ferris, R.L. Preclinical immunoPET/CT imaging using Zr-89-labeled anti-PD-L1 monoclonal antibody for assessing radiation-induced PD-L1 upregulation in head and neck cancer and melanoma. *Oncoimmunology* **2017**, *6*, e1329071. [[CrossRef](#)]
70. Christensen, C.; Kristensen, L.K.; Alfsen, M.Z.; Nielsen, C.H.; Kjaer, A. Quantitative PET imaging of PD-L1 expression in xenograft and syngeneic tumour models using a site-specifically labelled PD-L1 antibody. *Eur. J. Nucl. Med. Mol. Imaging* **2019**, *47*, 1302–1313. [[CrossRef](#)]
71. Lv, G.; Sun, X.; Qiu, L.; Sun, Y.; Li, K.; Liu, Q.; Zhao, Q.; Qin, S.; Lin, J. PET Imaging of Tumor PD-L1 Expression with a Highly Specific Nonblocking Single-Domain Antibody. *J. Nucl. Med.* **2019**, *61*, 117–122. [[CrossRef](#)]
72. Rubins, D.J.; Meng, X.; McQuade, P.; Klimas, M.; Getty, K.; Lin, S.-A.; Connolly, B.M.; O'Malley, S.S.; Haley, H.; Purcell, M.; et al. In Vivo Evaluation and Dosimetry Estimate for a High Affinity Affibody PET Tracer Targeting PD-L1. *Mol. Imaging Biol.* **2020**, *23*, 241–249. [[CrossRef](#)]
73. De Silva, R.A.; Kumar, D.; Lisok, A.; Chatterjee, S.; Wharram, B.; Rao, K.V.; Mease, R.; Dannals, R.F.; Pomper, M.G.; Nimmagadda, S. Peptide-Based ⁶⁸Ga-PET Radiotracer for Imaging PD-L1 Expression in Cancer. *Mol. Pharm.* **2018**, *15*, 3946–3952. [[CrossRef](#)]
74. Lesniak, W.G.; Mease, R.C.; Chatterjee, S.; Kumar, D.; Lisok, A.; Wharram, B.; Kalagadda, V.R.; Emens, L.A.; Pomper, M.G.; Nimmagadda, S. Development of [¹⁸F]FPy-WL12 as a PD-L1 Specific PET Imaging Peptide. *Mol. Imaging* **2019**, *18*, 1536012119852189. [[CrossRef](#)]
75. Mayer, A.T.; Natarajan, A.; Gordon, S.R.; Maute, R.L.; McCracken, M.N.; Ring, A.M.; Weissman, I.L.; Gambhir, S.S. Practical Immuno-PET Radiotracer Design Considerations for Human Immune Checkpoint Imaging. *J. Nucl. Med.* **2017**, *58*, 538–546. [[CrossRef](#)]
76. Truillet, C.; Oh, H.L.J.; Yeo, S.P.; Lee, C.Y.; Huynh, L.T.; Wei, J.; Parker, M.F.L.; Blakely, C.; Sevillano, N.; Wang, Y.H.; et al. Imaging PD-L1 Expression with ImmunoPET. *Bioconjug. Chem.* **2018**, *29*, 96–103. [[CrossRef](#)] [[PubMed](#)]
77. Xu, M.; Han, Y.; Liu, G.; Xu, Y.; Duan, D.; Liu, H.; Du, F.; Luo, P.; Liu, Z. Preclinical Study of a Fully Human Anti-PD-L1 Antibody as a Theranostic Agent for Cancer Immunotherapy. *Mol. Pharm.* **2018**, *15*, 4426–4433. [[CrossRef](#)] [[PubMed](#)]
78. Wissler, H.L.; Ehlerding, E.B.; Lyu, Z.; Zhao, Y.; Zhang, S.; Eshraghi, A.; Buuh, Z.Y.; McGuth, J.C.; Guan, Y.; Engle, J.W.; et al. Site-Specific Immuno-PET Tracer to Image PD-L1. *Mol. Pharm.* **2019**, *16*, 2028–2036. [[CrossRef](#)] [[PubMed](#)]
79. Li, D.; Cheng, S.; Zou, S.; Zhu, D.; Zhu, T.; Wang, P.; Zhu, X. Immuno-PET Imaging of ⁸⁹Zr Labeled Anti-PD-L1 Domain Antibody. *Mol. Pharm.* **2018**, *15*, 1674–1681. [[CrossRef](#)]
80. Li, D.; Zou, S.; Cheng, S.; Song, S.; Wang, P.; Zhu, X. Monitoring the Response of PD-L1 Expression to Epidermal Growth Factor Receptor Tyrosine Kinase Inhibitors in Nonsmall-Cell Lung Cancer Xenografts by Immuno-PET Imaging. *Mol. Pharm.* **2019**, *16*, 3469–3476. [[CrossRef](#)]
81. Miao, Y.; Lv, G.; Chen, Y.; Qiu, L.; Xie, M.; Lin, J. One-Step Radiosynthesis and Initial Evaluation of a Small Molecule PET Tracer for PD-L1 Imaging. *Bioorg. Med. Chem. Lett.* **2020**, *30*, 127572. [[CrossRef](#)]
82. Vento, J.; Mulgaonkar, A.; Woolford, L.; Nham, K.; Christie, A.; Bagrodia, A.; De Leon, A.D.; Hannan, R.; Bowman, I.; McKay, R.M.; et al. PD-L1 detection using ⁸⁹Zr-atezolizumab immuno-PET in renal cell carcinoma tumorgrafts from a patient with favorable nivolumab response. *J. Immunother. Cancer* **2019**, *7*, 144. [[CrossRef](#)]
83. Van Der Veen, E.L.; Giesen, D.; Jong, L.P.-D.; Jorritsma-Smit, A.; Vries, E.G.E.D.; Hooge, M.N.L.-D. ⁸⁹Zr-pembrolizumab biodistribution is influenced by PD-1-mediated uptake in lymphoid organs. *J. Immunother. Cancer* **2020**, *8*, e000938. [[CrossRef](#)]

84. Li, W.; Wang, Y.; Rubins, D.; Bennacef, I.; Holahan, M.; Haley, H.; Purcell, M.; Gantert, L.; Hseih, S.C.; Judo, M.; et al. PET/CT Imaging of 89Zr-N-sucDf-Pembrolizumab in Healthy Cynomolgus Monkeys. *Mol. Imaging Biol.* **2020**, *23*, 250–259. [[CrossRef](#)]
85. Cole, E.L.; Kim, J.; Donnelly, D.J.; Smith, R.A.; Cohen, D.; Lafont, V.; Morin, P.E.; Huang, R.Y.-C.; Chow, P.L.; Hayes, W.; et al. Radiosynthesis and preclinical PET evaluation of 89Zr-nivolumab (BMS-936558) in healthy non-human primates. *Bioorg. Med. Chem.* **2017**, *25*, 5407–5414. [[CrossRef](#)]
86. England, C.G.; Jiang, D.; Ehlerding, E.B.; Rekoske, B.T.; Ellison, P.A.; Hernandez, R.; Barnhart, T.E.; McNeel, D.G.; Huang, P.; Cai, W. 89Zr-labeled nivolumab for imaging of T-cell infiltration in a humanized murine model of lung cancer. *Eur. J. Nucl. Med. Mol. Imaging* **2018**, *45*, 110–120. [[CrossRef](#)] [[PubMed](#)]
87. Ehlerding, E.B.; Lee, H.J.; Jiang, D.; A Ferreira, C.; Zahm, C.D.; Huang, P.; Engle, J.W.; McNeel, D.G.; Cai, W. Antibody and fragment-based PET imaging of CTLA-4+ T-cells in humanized mouse models. *Am. J. Cancer Res.* **2019**, *9*, 53–63.
88. Ehlerding, E.B.; England, C.G.; Majewski, R.L.; Valdovinos, H.F.; Jiang, D.; Liu, G.; McNeel, D.G.; Nickles, R.J.; Cai, W. ImmunoPET Imaging of CTLA-4 Expression in Mouse Models of Non-small Cell Lung Cancer. *Mol. Pharm.* **2017**, *14*, 1782–1789. [[CrossRef](#)] [[PubMed](#)]
89. Rosenberg, S.A.; Restifo, N.P.; Yang, J.C.; Morgan, R.A.; Dudley, M.E. Adoptive cell transfer: A clinical path to effective cancer immunotherapy. *Nat. Rev. Cancer* **2008**, *8*, 299–308. [[CrossRef](#)] [[PubMed](#)]
90. Baggio, L.; Laureano, Á.M.; Silla, L.M.D.R.; Lee, D.A. Natural killer cell adoptive immunotherapy: Coming of age. *Clin. Immunol.* **2017**, *177*, 3–11. [[CrossRef](#)] [[PubMed](#)]
91. Sato, N.; Stringaris, K.; Davidson-Moncada, J.K.; Reger, R.; Adler, S.S.; Dunbar, C.; Choyke, P.L.; Childs, R.W. In Vivo Tracking of Adoptively Transferred Natural Killer Cells in Rhesus Macaques Using 89Zirconium-Oxine Cell Labeling and PET Imaging. *Clin. Cancer Res.* **2020**, *26*, 2573–2581. [[CrossRef](#)]
92. Shaffer, T.M.; Aalipour, A.; Schürch, C.M.; Gambhir, S.S. PET Imaging of the Natural Killer Cell Activation Receptor NKp30. *J. Nucl. Med.* **2020**, *61*, 1348–1354. [[CrossRef](#)] [[PubMed](#)]
93. Hmadcha, A.; Martin-Montalvo, A.; Gauthier, B.R.; Soria, B.; Capilla-Gonzalez, V. Therapeutic Potential of Mesenchymal Stem Cells for Cancer Therapy. *Front. Bioeng. Biotechnol.* **2020**, *8*, 43. [[CrossRef](#)] [[PubMed](#)]
94. Belderbos, S.; González-Gómez, M.A.; Cleeren, F.; Wouters, J.; Piñeiro, Y.; Deroose, C.M.; Coosemans, A.; Gsell, W.; Bormans, G.; Rivas, J.; et al. Simultaneous in vivo PET/MRI using fluorine-18 labeled Fe3O4@Al(OH)3 nanoparticles: Comparison of nanoparticle and nanoparticle-labeled stem cell distribution. *EJNMMI Res.* **2020**, *10*, 1–13. [[CrossRef](#)]
95. Keu, K.V.; Witney, T.H.; Yaghoubi, S.; Rosenberg, J.; Kurien, A.; Magnusson, R.; Williams, J.; Habte, F.; Wagner, J.R.; Forman, S.; et al. Reporter gene imaging of targeted T cell immunotherapy in recurrent glioma. *Sci. Transl. Med.* **2017**, *9*, 373. [[CrossRef](#)] [[PubMed](#)]
96. Volpe, A.; Lang, C.; Lim, L.; Man, F.; Kurtys, E.; Ashmore-Harris, C.; Johnson, P.; Skourti, E.; de Rosales, R.T.M.; Fruhwirth, G.O. Spatiotemporal PET Imaging Reveals Differences in CAR-T Tumor Retention in Triple-Negative Breast Cancer Models. *Mol. Ther.* **2020**, *28*, 2271–2285. [[CrossRef](#)]
97. Minn, I.; Huss, D.J.; Ahn, H.H.; Chinn, T.M.; Park, A.; Jones, J.; Brummet, M.; Rowe, S.P.; Sysa-Shah, P.; Du, Y.; et al. Imaging CAR T cell therapy with PSMA-targeted positron emission tomography. *Sci. Adv.* **2019**, *5*, eaaw5096. [[CrossRef](#)] [[PubMed](#)]
98. Arndt, C.; Feldmann, A.; Koristka, S.; Schäfer, M.; Bergmann, R.; Mitwasi, N.; Berndt, N.; Bachmann, D.; Kegler, A.; Schmitz, M.; et al. A theranostic PSMA ligand for PET imaging and retargeting of T cells expressing the universal chimeric antigen receptor UniCAR. *Oncoimmunology* **2019**, *8*, 1659095. [[CrossRef](#)] [[PubMed](#)]
99. Kumar, S.; Singh, S.K.; Rana, B.; Rana, A. Tumor-infiltrating CD8+ T cell antitumor efficacy and exhaustion: Molecular insights. *Drug Discov. Today* **2021**. [[CrossRef](#)]
100. Wei, S.C.; Duffy, C.R.; Allison, J.P. Fundamental Mechanisms of Immune Checkpoint Blockade Therapy. *Cancer Discov.* **2018**, *8*, 1069–1086. [[CrossRef](#)]
101. Gooden, M.J.M.; De Bock, G.H.; Leffers, N.; Daemen, T.; Nijman, H.W. The prognostic influence of tumour-infiltrating lymphocytes in cancer: A systematic review with meta-analysis. *Br. J. Cancer* **2011**, *105*, 93–103. [[CrossRef](#)]
102. Tavaré, R.; McCracken, M.N.; Zettlitz, K.A.; Knowles, S.M.; Salazar, F.B.; Olafsen, T.; Witte, O.N.; Wu, A.M. Engineered antibody fragments for immuno-PET imaging of endogenous CD8+ T cells in vivo. *Proc. Natl. Acad. Sci. USA* **2014**, *111*, 1108–1113. [[CrossRef](#)]
103. Kristensen, L.K.; Fröhlich, C.; Christensen, C.; Melander, M.C.; Poulsen, T.T.; Galler, G.R.; Lantto, J.; Horak, I.D.; Kragh, M.; Nielsen, C.H.; et al. CD4+ and CD8a+ PET imaging predicts response to novel PD-1 checkpoint inhibitor: Studies of Sym021 in syngeneic mouse cancer models. *Theranostics* **2019**, *9*, 8221–8238. [[CrossRef](#)]
104. Griessinger, C.M.; Olafsen, T.; Mascioni, A.; Jiang, Z.K.; Zamilpa, C.; Jia, F.; Torgov, M.; Romero, J.M.; Marchioni, F.; Satpayev, D.; et al. The PET-Tracer 89Zr-Df-IAB22M2C Enables Monitoring of Intratumoral CD8 T-cell Infiltrates in Tumor-Bearing Humanized Mice after T-cell Bispecific Antibody Treatment. *Cancer Res.* **2020**, *80*, 2903–2913. [[CrossRef](#)]
105. Kristensen, L.K.; Christensen, C.; Alfsen, M.Z.; Cold, S.; Nielsen, C.H.; Kjaer, A. Monitoring CD8a+ T Cell Responses to Radiotherapy and CTLA-4 Blockade Using [64Cu]NOTA-CD8a PET Imaging. *Mol. Imaging Biol.* **2020**, *22*, 1021–1030. [[CrossRef](#)]
106. Seo, J.W.; Tavaré, R.; Mahakian, L.M.; Silvestrini, M.T.; Tam, S.; Ingham, E.S.; Salazar, F.B.; Borowsky, A.D.; Wu, A.M.; Ferrara, K.W. CD8+ T-Cell Density Imaging with 64Cu-Labeled Cys-Diabody Informs Immunotherapy Protocols. *Clin. Cancer Res.* **2018**, *24*, 4976–4987. [[CrossRef](#)] [[PubMed](#)]

107. Rashidian, M.; Ingram, J.R.; Dougan, M.; Dongre, A.; Whang, K.A.; LeGall, C.; Cragolini, J.J.; Bieri, B.; Gostissa, M.; Gorman, J.; et al. Predicting the response to CTLA-4 blockade by longitudinal noninvasive monitoring of CD8 T cells. *J. Exp. Med.* **2017**, *214*, 2243–2255. [[CrossRef](#)] [[PubMed](#)]
108. Rashidian, M.; LaFleur, M.W.; Verschoor, V.L.; Dongre, A.; Zhang, Y.; Nguyen, T.H.; Kolifraath, S.; Aref, A.R.; Lau, C.J.; Paweletz, C.P.; et al. Immuno-PET identifies the myeloid compartment as a key contributor to the outcome of the antitumor response under PD-1 blockade. *Proc. Natl. Acad. Sci. USA* **2019**, *116*, 16971–16980. [[CrossRef](#)]
109. Namavari, M.; Chang, Y.F.; Kusler, B.; Yaghoubi, S.; Mitchell, B.S.; Gambhir, S.S. Synthesis of 2'-Deoxy-2'-[18F]Fluoro-9-β-D-Arabinofuranosylguanine: A Novel Agent for Imaging T-Cell Activation with PET. *Mol. Imaging Biol.* **2011**, *13*, 812–818. [[CrossRef](#)] [[PubMed](#)]
110. Levi, J.; Lam, T.; Goth, S.R.; Yaghoubi, S.; Bates, J.; Ren, G.; Jivan, S.; Huynh, T.L.; Blecha, J.E.; Khattri, R.; et al. Imaging of Activated T Cells as an Early Predictor of Immune Response to Anti-PD-1 Therapy. *Cancer Res.* **2019**, *79*, 3455–3465. [[CrossRef](#)]
111. Hutloff, A.; Dittrich, A.M.; Beier, K.C.; Eljaschewitsch, B.; Kraft, R.; Anagnostopoulos, I.; Kroczek, R.A. ICOS is an inducible T-cell co-stimulator structurally and functionally related to CD28. *Nat. Cell Biol.* **1999**, *397*, 263–266. [[CrossRef](#)]
112. Xiao, Z.; Mayer, A.T.; Nobashi, T.W.; Gambhir, S.S. ICOS Is an Indicator of T-cell-Mediated Response to Cancer Immunotherapy. *Cancer Res.* **2020**, *80*, 3023–3032. [[CrossRef](#)] [[PubMed](#)]
113. Opitz, C.A.; Patterson, L.F.S.; Mohapatra, S.R.; Dewi, D.L.; Sadik, A.; Platten, M.; Trump, S. The therapeutic potential of targeting tryptophan catabolism in cancer. *Br. J. Cancer* **2020**, *122*, 30–44. [[CrossRef](#)] [[PubMed](#)]
114. Kim, H.Y.; Li, R.; Ng, T.S.C.; Courties, G.; Rodell, C.B.; Prytyskach, M.; Kohler, R.H.; Pittet, M.J.; Nahrendorf, M.; Weissleder, R.; et al. Quantitative Imaging of Tumor-Associated Macrophages and Their Response to Therapy Using 64Cu-Labeled Macrin. *ACS Nano* **2018**, *12*, 12015–12029. [[CrossRef](#)] [[PubMed](#)]
115. Sørensen, M.D.; Dahlrot, R.H.; Boldt, H.B.; Hansen, S.; Kristensen, B.W. Tumour-associated microglia/macrophages predict poor prognosis in high-grade gliomas and correlate with an aggressive tumour subtype. *Neuropathol. Appl. Neurobiol.* **2018**, *44*, 185–206. [[CrossRef](#)]
116. Nigam, S.; McCarl, L.; Kumar, R.; Edinger, R.S.; Kurland, B.F.; Anderson, C.J.; Panigrahy, A.; Kohanbash, G.; Edwards, W.B. Preclinical ImmunoPET Imaging of Glioblastoma-Infiltrating Myeloid Cells Using Zirconium-89 Labeled Anti-CD11b Antibody. *Mol. Imaging Biol.* **2020**, *22*, 685–694. [[CrossRef](#)] [[PubMed](#)]
117. Mason, C.A.; Kossatz, S.; Carter, L.M.; Pirovano, G.; Brand, C.; Guru, N.; Pérez-Medina, C.; Lewis, J.S.; Mulder, W.J.M.; Reiner, T. An 89Zr-HDL PET Tracer Monitors Response to a CSF1R Inhibitor. *J. Nucl. Med.* **2020**, *61*, 433–436. [[CrossRef](#)]
118. Goggi, J.L.; Hartimath, S.V.; Hwang, Y.; Tan, Y.X.; Khanapur, S.; Ramasamy, B.; Jiang, L.; Yong, F.F.; Cheng, P.; Tan, P.W.; et al. Examining Immunotherapy Response Using Multiple Radiotracers. *Mol. Imaging Biol.* **2020**, *22*, 993–1002. [[CrossRef](#)]
119. Larimer, B.M.; Wehrenberg-Klee, E.; Caraballo, A.; Mahmood, U. Quantitative CD3 PET Imaging Predicts Tumor Growth Response to Anti-CTLA-4 Therapy. *J. Nucl. Med.* **2016**, *57*, 1607–1611. [[CrossRef](#)]
120. Baeuerle, P.A.; Reinhardt, C. Bispecific T-Cell Engaging Antibodies for Cancer Therapy. *Cancer Res.* **2009**, *69*, 4941–4944. [[CrossRef](#)]
121. Kujawski, M.; Li, L.; Bhattacharya, S.; Wong, P.; Lee, W.-H.; Williams, L.; Li, H.; Chea, J.; Poku, K.; Bowles, N.; et al. Generation of dual specific bivalent BiTEs (dbBispecific T-cell engaging antibodies) for cellular immunotherapy. *BMC Cancer* **2019**, *19*, 882. [[CrossRef](#)] [[PubMed](#)]
122. Malek, T.R.; Castro, I. Interleukin-2 Receptor Signaling: At the Interface between Tolerance and Immunity. *Immunity* **2010**, *33*, 153–165. [[CrossRef](#)] [[PubMed](#)]
123. Di Galleonardo, V.; Signore, A.; Glaudemans, A.W.J.M.; Dierckx, R.A.J.O.; De Vries, E.F.J. N-(4-18F-Fluorobenzoyl)Interleukin-2 for PET of Human-Activated T Lymphocytes. *J. Nucl. Med.* **2012**, *53*, 679–686. [[CrossRef](#)]
124. Hartimath, S.V.; Draghiciu, O.; Van De Wall, S.; Manuelli, V.; Dierckx, R.A.J.O.; Nijman, H.W.; Daemen, T.; De Vries, E.F.J. Noninvasive monitoring of cancer therapy induced activated T cells using [18F]FB-IL-2 PET imaging. *Oncoimmunology* **2017**, *6*, e1248014. [[CrossRef](#)]
125. Van Der Veen, E.L.; Antunes, I.F.; Maarsingh, P.; Hessels-Scheper, J.; Zijlma, R.; Boersma, H.H.; Jorritsma-Smit, A.; Hospers, G.A.P.; De Vries, E.G.E.; Hooge, M.N.L.-D.; et al. Clinical-grade N-(4-[18F]fluorobenzoyl)-interleukin-2 for PET imaging of activated T-cells in humans. *EJNMMI Radiopharm. Chem.* **2019**, *4*, 1–15. [[CrossRef](#)]
126. Zanetti, M. Tapping CD4 T Cells for Cancer Immunotherapy: The Choice of Personalized Genomics. *J. Immunol.* **2015**, *194*, 2049–2056. [[CrossRef](#)]
127. Tavaré, R.; McCracken, M.N.; Zettlitz, K.A.; Salazar, F.B.; Olafsen, T.; Witte, O.N.; Wu, A.M. Immuno-PET of Murine T Cell Reconstitution Postadoptive Stem Cell Transplantation Using Anti-CD4 and Anti-CD8 Cys-Diabodies. *J. Nucl. Med.* **2015**, *56*, 1258–1264. [[CrossRef](#)]
128. Freise, A.C.; Zettlitz, K.A.; Salazar, F.B.; Lu, X.; Tavaré, R.; Wu, A.M. ImmunoPET Imaging of Murine CD4+ T Cells Using Anti-CD4 Cys-Diabody: Effects of Protein Dose on T Cell Function and Imaging. *Mol. Imaging Biol.* **2017**, *19*, 599–609. [[CrossRef](#)]
129. Kaira, K.; Kuji, I.; Kagamu, H. Value of 18F-FDG-PET to predict PD-L1 expression and outcomes of PD-1 inhibition therapy in human cancers. *Cancer Imaging* **2021**, *21*, 762. [[CrossRef](#)] [[PubMed](#)]
130. Cho, S.Y.; Huff, D.T.; Jeraj, R.; Albertini, M.R. FDG PET/CT for Assessment of Immune Therapy: Opportunities and Understanding Pitfalls. *Semin. Nucl. Med.* **2020**, *50*, 518–531. [[CrossRef](#)] [[PubMed](#)]

131. Ayati, N.; Sadeghi, R.; Kiamanesh, Z.; Lee, S.T.; Zakavi, S.R.; Scott, A.M. The value of 18F-FDG PET/CT for predicting or monitoring immunotherapy response in patients with metastatic melanoma: A systematic review and meta-analysis. *Eur. J. Nucl. Med. Mol. Imaging* **2020**, *48*, 428–448. [CrossRef] [PubMed]
132. Irvani, A.; Hicks, R.J. Imaging the Cancer Immune Environment and Its Response to Pharmacologic Intervention, Part 1: The Role of 18F-FDG PET/CT. *J. Nucl. Med.* **2020**, *61*, 943–950. [CrossRef] [PubMed]
133. Beer, L.; Hochmair, M.; Haug, A.R.; Schwabel, B.; Kifjak, D.; Wadsak, W.; Fureder, T.; Fabikan, H.; Fazekas, A.; Schwab, S.; et al. Comparison of RECIST, iRECIST, and PERCIST for the Evaluation of Response to PD-1/PD-L1 Blockade Therapy in Patients With Non-Small Cell Lung Cancer. *Clin. Nucl. Med.* **2019**, *44*, 535–543. [CrossRef] [PubMed]
134. Mulkey, F.; Theoret, M.R.; Keegan, P.; Pazdur, R.; Sridhara, R. Comparison of iRECIST versus RECIST V.1.1 in patients treated with an anti-PD-1 or PD-L1 antibody: Pooled FDA analysis. *J. Immunother. Cancer* **2020**, *8*, e000146. [CrossRef]
135. Tazdait, M.; Mezquita, L.; Lahmar, J.; Ferrara, R.; Bidault, F.; Ammari, S.; Balleyguier, C.; Planchard, D.; Gazzah, A.; Soria, J.C.; et al. Patterns of responses in metastatic NSCLC during PD-1 or PDL-1 inhibitor therapy: Comparison of RECIST 1.1, irRECIST and iRECIST criteria. *Eur. J. Cancer* **2018**, *88*, 38–47. [CrossRef]
136. Cheson, B.D.; Ansell, S.; Schwartz, L.; Gordon, L.I.; Advani, R.; Jacene, H.A.; Hoos, A.; Barrington, S.F.; Armand, P. Refinement of the Lugano Classification lymphoma response criteria in the era of immunomodulatory therapy. *Blood* **2016**, *128*, 2489–2496. [CrossRef]
137. Ito, K.; Teng, R.; Schöder, H.; Humm, J.L.; Ni, A.; Michaud, L.; Nakajima, R.; Yamashita, R.; Wolchok, J.D.; Weber, W.A. 18F-FDG PET/CT for Monitoring of Ipilimumab Therapy in Patients with Metastatic Melanoma. *J. Nucl. Med.* **2019**, *60*, 335–341. [CrossRef]
138. Anwar, H.; Sachpekidis, C.; Winkler, J.; Kopp-Schneider, A.; Haberkorn, U.; Hassel, J.C.; Dimitrakopoulou-Strauss, A. Absolute number of new lesions on 18F-FDG PET/CT is more predictive of clinical response than SUV changes in metastatic melanoma patients receiving ipilimumab. *Eur. J. Nucl. Med. Mol. Imaging* **2018**, *45*, 376–383. [CrossRef]
139. Hodi, F.S.; Ballinger, M.; Lyons, B.; Soria, J.C.; Nishino, M.; Tabernero, J.; Powles, T.; Smith, D.; Hoos, A.; McKenna, C.; et al. Immune-Modified Response Evaluation Criteria In Solid Tumors (imRECIST): Refining Guidelines to Assess the Clinical Benefit of Cancer Immunotherapy. *J. Clin. Oncol.* **2018**, *36*, 850–858. [CrossRef] [PubMed]
140. Wolchok, J.D.; Hoos, A.; O'Day, S.; Weber, J.S.; Hamid, O.; Lebbé, C.; Maio, M.; Binder, M.; Bohnsack, O.; Nichol, G.; et al. Guidelines for the Evaluation of Immune Therapy Activity in Solid Tumors: Immune-Related Response Criteria. *Clin. Cancer Res.* **2009**, *15*, 7412–7420. [CrossRef] [PubMed]
141. Seymour, L.; Bogaerts, J.; Perrone, A.; Ford, R.; Schwartz, L.H.; Mandrekar, S.; Lin, N.U.; Litière, S.; Dancey, J.; Chen, A.; et al. iRECIST: Guidelines for response criteria for use in trials testing immunotherapeutics. *Lancet Oncol.* **2017**, *18*, e143–e152. [CrossRef]
142. Costa, L.B.; Queiroz, M.A.; Barbosa, F.G.; Nunes, R.F.; Zaniboni, E.C.; Ruiz, M.M.; Jardim, D.; Marin, J.F.G.; Cerri, G.G.; Buchpiguel, C.A. Reassessing Patterns of Response to Immunotherapy with PET: From Morphology to Metabolism. *Radiographics* **2021**, *41*, 120–143. [CrossRef] [PubMed]
143. Park, H.J.; Kim, K.W.; Pyo, J.; Suh, C.H.; Yoon, S.; Hatabu, H.; Nishino, M. Incidence of Pseudoprogression during Immune Checkpoint Inhibitor Therapy for Solid Tumors: A Systematic Review and Meta-Analysis. *Radiology* **2020**, *297*, 87–96. [CrossRef] [PubMed]
144. Seban, R.D.; Nemer, J.S.; Marabelle, A.; Yeh, R.; Deutsch, E.; Ammari, S.; Moya-Plana, A.; Mokrane, F.Z.; Gartrell, R.D.; Finkel, G.; et al. Prognostic and theranostic 18F-FDG PET biomarkers for anti-PD1 immunotherapy in metastatic melanoma: Association with outcome and transcriptomics. *Eur. J. Nucl. Med. Mol. Imaging* **2019**, *46*, 2298–2310. [CrossRef] [PubMed]
145. Laudicella, R.; Comelli, A.; Stefano, A.; Szostek, M.; Crocè, L.; Vento, A.; Spataro, A.; Comis, A.D.; La Torre, F.; Gaeta, M.; et al. Artificial Neural Networks in Cardiovascular Diseases and its Potential for Clinical Application in Molecular Imaging. *Curr. Radiopharm.* **2020**, *13*. [CrossRef]
146. Lambin, P.; Leijenaar, R.T.H.; Deist, T.M.; Peerlings, J.; De Jong, E.E.C.; Van Timmeren, J.; Sanduleanu, S.; Larue, R.T.H.M.; Even, A.J.G.; Jochems, A.; et al. Radiomics: The Bridge between Medical Imaging and Personalized Medicine. Available online: <https://www.ncbi.nlm.nih.gov/pubmed/?term=Lambin++Radiomics%3A+the+bridge+between+medical+imaging+and+personalized+medicine> (accessed on 7 February 2020).
147. Mayerhoefer, M.E.; Materka, A.; Langs, G.; Häggström, I.; Szczypiński, P.; Gibbs, P.; Cook, G. Introduction to Radiomics. *J. Nucl. Med.* **2020**, *61*, 488–495. [CrossRef]
148. Lee, D.Y.; Kim, Y.I. Prognostic Value of Maximum Standardized Uptake Value in 68Ga-Somatostatin Receptor Positron Emission Tomography for Neuroendocrine Tumors: A Systematic Review and Meta-analysis. *Clin. Nucl. Med.* **2019**, *44*, 777–783. [CrossRef]
149. Valentinuzzi, D.; Vrankar, M.; Boc, N.; Ahac, V.; Zupancic, Z.; Unk, M.; Skalic, K.; Zagar, I.; Studen, A.; Simoncic, U.; et al. [18F]FDG PET immunotherapy radiomics signature (iRADIOMICS) predicts response of non-small-cell lung cancer patients treated with pembrolizumab. *Radiol. Oncol.* **2020**, *54*, 285–294. [CrossRef]
150. Polverari, G.; Ceci, F.; Bertaglia, V.; Reale, M.L.; Rampado, O.; Gallio, E.; Passera, R.; Liberini, V.; Scapoli, P.; Arena, V.; et al. 18F-FDG Pet Parameters and Radiomics Features Analysis in Advanced Nsclc Treated with Immunotherapy as Predictors of Therapy Response and Survival. *Cancers* **2020**, *12*, 1163. [CrossRef]
151. Mu, W.; Tunali, I.; Gray, J.E.; Qi, J.; Schabath, M.B.; Gillies, R.J. Radiomics of 18F-FDG PET/CT images predicts clinical benefit of advanced NSCLC patients to checkpoint blockade immunotherapy. *Eur. J. Nucl. Med. Mol. Imaging* **2019**, *47*, 1168–1182. [CrossRef]

152. Park, S.; Ha, S.; Lee, S.-H.; Paeng, J.C.; Keam, B.; Kim, T.M.; Kim, D.-W.; Heo, D.S. Intratumoral heterogeneity characterized by pretreatment PET in non-small cell lung cancer patients predicts progression-free survival on EGFR tyrosine kinase inhibitor. *PLoS ONE* **2018**, *13*, e0189766. [[CrossRef](#)]
153. Parvez, A.; Tau, N.; Hussey, D.; Maganti, M.; Metser, U. 18F-FDG PET/CT metabolic tumor parameters and radiomics features in aggressive non-Hodgkin's lymphoma as predictors of treatment outcome and survival. *Ann. Nucl. Med.* **2018**, *32*, 410–416. [[CrossRef](#)] [[PubMed](#)]
154. Aide, N.; Fruchart, C.; Nganoa, C.; Gac, A.C.; Lasnon, C. Baseline 18F-FDG PET radiomic features as predictors of 2-year event-free survival in diffuse large B cell lymphomas treated with immunochemotherapy. *Eur. Radiol.* **2020**, *30*, 4623–4632. [[CrossRef](#)] [[PubMed](#)]
155. Prigent, K.; Lasnon, C.; Ezine, E.; Janson, M.; Coudrais, N.; Joly, E.; Césaire, L.; Stefan, A.; Depontville, M.; Aide, N. Assessing immune organs on 18F-FDG PET/CT imaging for therapy monitoring of immune checkpoint inhibitors: Inter-observer variability, prognostic value and evolution during the treatment course of melanoma patients. *Eur. J. Nucl. Med. Mol. Imaging* **2021**. [[CrossRef](#)]
156. Basler, L.; Gabryś, H.S.; Hogan, S.A.; Pavic, M.; Bogowicz, M.; Vuong, D.; Tanadini-Lang, S.; Förster, R.; Kudura, K.; Huellner, M.W.; et al. Radiomics, Tumor Volume, and Blood Biomarkers for Early Prediction of Pseudoprogression in Patients with Metastatic Melanoma Treated with Immune Checkpoint Inhibition. *Clin. Cancer Res.* **2020**, *26*, 4414–4425. [[CrossRef](#)] [[PubMed](#)]
157. Koyasu, S.; Nishio, M.; Isoda, H.; Nakamoto, Y.; Togashi, K. Usefulness of gradient tree boosting for predicting histological subtype and EGFR mutation status of non-small cell lung cancer on 18F FDG-PET/CT. *Ann. Nucl. Med.* **2020**, *34*, 49–57. [[CrossRef](#)] [[PubMed](#)]
158. Zhang, J.; Zhao, X.; Zhao, Y.; Zhang, J.; Zhang, Z.; Wang, J.; Wang, Y.; Dai, M.; Han, J. Value of pre-therapy 18F-FDG PET/CT radiomics in predicting EGFR mutation status in patients with non-small cell lung cancer. *Eur. J. Nucl. Med. Mol. Imaging* **2020**, *47*, 1137–1146. [[CrossRef](#)] [[PubMed](#)]
159. Li, X.; Yin, G.; Zhang, Y.; Dai, D.; Liu, J.; Chen, P.; Zhu, L.; Ma, W.; Xu, W. Predictive Power of a Radiomic Signature Based on 18F-FDG PET/CT Images for EGFR Mutational Status in NSCLC. *Front. Oncol.* **2019**, *9*, 1062. [[CrossRef](#)]
160. Jiang, M.; Zhang, Y.; Xu, J.; Ji, M.; Guo, Y.; Guo, Y.; Xiao, J.; Yao, X.; Shi, H.; Zeng, M. Assessing EGFR gene mutation status in non-small cell lung cancer with imaging features from PET/CT. *Nucl. Med. Commun.* **2019**, *40*, 842–849. [[CrossRef](#)]
161. Jiang, M.; Sun, D.; Guo, Y.; Guo, Y.; Xiao, J.; Wang, L.; Yao, X. Assessing PD-L1 Expression Level by Radiomic Features From PET/CT in Nonsmall Cell Lung Cancer Patients: An Initial Result. *Acad. Radiol.* **2020**, *27*, 171–179. [[CrossRef](#)]
162. Park, C.; Na, K.J.; Choi, H.; Ock, C.Y.; Ha, S.; Kim, M.; Park, S.; Keam, B.; Kim, T.M.; Paeng, J.C.; et al. Tumor immune profiles noninvasively estimated by FDG PET with deep learning correlate with immunotherapy response in lung adenocarcinoma. *Theranostics* **2020**, *10*, 10838–10848. [[CrossRef](#)] [[PubMed](#)]
163. Kather, J.N.; Suarez-Carmona, M.; Charoentong, P.; Weis, C.A.; Hirsch, D.; Bankhead, P.; Horning, M.; Ferber, D.; Kel, I.; Herpel, E.; et al. Topography of cancer-associated immune cells in human solid tumors. *Elife* **2018**, *7*, e36967. [[CrossRef](#)] [[PubMed](#)]
164. Pietrobon, V.; Cesano, A.; Marincola, F.; Kather, J.N. Next Generation Imaging Techniques to Define Immune Topographies in Solid Tumors. *Front. Immunol.* **2021**, *11*, 3519. [[CrossRef](#)] [[PubMed](#)]